



1 Arctic tropospheric ozone: assessment of current knowledge 2 and model performance

3 Cynthia H. Whaley¹, Kathy S. Law², Jens Lienggaard Hjorth³, Henrik Skov³, Stephen R.
4 Arnold⁴, Joakim Langner⁵, Jakob Boyd Pernov^{3,†}, Rong-You Chien⁶, Jesper H. Christensen³,
5 Makoto Deushi¹¹, Xinyi Dong⁶, Gregory Faluvegi^{7,8}, Mark Flanner⁹, Joshua S. Fu⁶, Michael
6 Gauss¹⁰, Ulas Im³, Louis Marelle², Tatsuo Onishi², Naga Oshima¹¹, David A. Plummer¹,
7 Luca Pozzoli^{12,*}, Jean-Christophe Raut², Ragnhild Skeie¹³, Manu A. Thomas⁵, Kostas
8 Tsigaridis⁸, Svetlana Tsyro¹⁰, Steven T. Turnock^{14,4}, Knut von Salzen¹, David W. Tarasick¹⁵

9 ¹Climate Research Division, Environment and Climate Change Canada, Victoria, BC, Canada

10 ²LATMOS/IPSL, Sorbonne Université, UVSQ, CNRS, Paris, France.

11 ³Department of Environmental Science/Interdisciplinary Centre for Climate Change, Aarhus University,
12 Frederiksborgvej 400, Roskilde, Denmark.

13 ⁴Institute for Climate and Atmospheric Science, School of Earth and Environment, University of Leeds, Leeds,
14 United Kingdom.

15 ⁵Swedish Meteorological and Hydrological Institute, Norrköping, Sweden.

16 ⁶University of Tennessee, Knoxville, Tennessee, United States.

17 ⁷NASA Goddard Institute for Space Studies, New York, NY, USA.

18 ⁸Center for Climate Systems Research, Columbia University; New York, USA.

19 ⁹Department of Climate and Space Sciences and Engineering, University of Michigan, Ann Arbor, MI, USA.

20 ¹⁰Norwegian Meteorological Institute, Oslo, Norway.

21 ¹¹Meteorological Research Institute, Japan Meteorological Agency, Tsukuba, Japan.

22 ¹²European Commission, Joint Research Centre, Ispra, Italy.

23 ¹³CICERO Center for International Climate and Environmental Research, Oslo, Norway.

24 ¹⁴Met Office Hadley Centre, Exeter, UK.

25 ¹⁵Air Quality Research Division, Environment and Climate Change Canada, Toronto, ON, Canada.

26 †Now at: Extreme Environments Research Laboratory, École Polytechnique fédérale de Lausanne, 1951 Sion,
27 Switzerland

28 *now at, FINCONS SPA, Via Torri Bianche 10, 20871 Vimercate, Italy

29

30 *Correspondence to:* Cynthia H. Whaley (cynthia.whaley@ec.gc.ca)

31 **Abstract.** As the third most important greenhouse gas (GHG) after CO₂ and methane, tropospheric ozone (O₃) is
32 also an air pollutant causing damage to human health and ecosystems. This study brings together recent research
33 on observations and modeling of tropospheric O₃ in the Arctic, a rapidly warming and sensitive environment. At
34 different locations in the Arctic, the observed surface O₃ seasonal cycles are quite different. Coastal Arctic
35 locations, for example, have a minimum in the springtime due to O₃ depletion events resulting from surface
36 bromine chemistry. In contrast, other Arctic locations have a maximum in the spring. The 12 state-of-the-art
37 models used in this study lack the surface halogen chemistry needed to simulate coastal Arctic surface O₃ depletion
38 in the springtime, however, the multi-model median (MMM) has accurate seasonal cycles at non-coastal Arctic
39 locations. There is a large amount of variability among models, which has been reported previously, and we show
40 that there continues to be no convergence among models, nor improved accuracy in simulating tropospheric O₃
41 and its precursor species. The MMM underestimates Arctic surface O₃ by 5% to 15% depending on the location.
42 The vertical distribution of tropospheric O₃ is studied from recent ozonesonde measurements and the models. The
43 models are highly variable, simulating free-tropospheric O₃ within a range of +/- 50% depending on the model
44 and the altitude. The MMM performs best, within +/- 8% at most locations and seasons. However, nearly all
45 models overestimate O₃ near the tropopause (~300 hPa or ~8 km), likely due to ongoing issues with
46 underestimating the altitude of the tropopause and excessive downward transport of stratospheric O₃ at high
47 latitudes. For example, the MMM is biased high by about 20% at Eureka. Observed and simulated O₃ precursors



48 (CO, NO_x and reservoir PAN) are evaluated throughout the troposphere. Models underestimate wintertime CO
49 everywhere, likely due to a combination of underestimating CO emissions and possibly overestimating OH.
50 Throughout the vertical profile (compared to aircraft measurements), the MMM underestimates both CO and NO_x
51 but overestimates PAN. Perhaps as a result of competing deficiencies, the MMM O₃ matches the observed O₃
52 reasonably well. Our findings suggest that despite model updates over the last decade, model results are as highly
53 variable as ever, and have not increased in accuracy for representing Arctic tropospheric.

54 **1 Introduction**

55 Tropospheric ozone (O₃) is the third most important greenhouse gas (GHG) after CO₂ and methane (IPCC, 2021),
56 and is an air pollutant causing damage to human health (WHO, 2013). It also causes damage to vegetation
57 following dry deposition to the surface (U.S. EPA, 2013). However, our knowledge about the sources and sinks
58 of tropospheric O₃ is still uncertain (AMAP, 2015; 2022; Gaudel et al., 2018), in particular in regions where fewer
59 observations exist, and where our understanding of key processes is still evolving. The Arctic is one such region
60 where few long-term measurements of O₃ exist and measurements of compounds that are important for producing
61 and destroying O₃ in the atmosphere are scarce at the surface and even more so in the free troposphere. Progress
62 has been made recently in terms of our understanding of certain processes and a picture is emerging about the
63 distribution of Arctic tropospheric O₃ as well as seasonal cycles and trends at different locations (e.g., Young et
64 al, 2018; Tarasick et al, 2019b). In particular, the connection between surface O₃ depletion episodes and halogens
65 is now well established (e.g., Simpson et al., 2007; Abbatt et al., 2012).

66 However, the role of natural cycles in the Arctic O₃ budget relative to O₃ produced from anthropogenic emissions
67 and how that relationship is changing in response to rapid warming in the Arctic are still uncertain. Arctic warming
68 and associated development in the Arctic are also driving changes in local anthropogenic emissions which could
69 already be leading to changes in the relative contributions of O₃ produced due to long-range transport of mid-
70 latitude anthropogenic emissions and O₃ produced from within or near-Arctic anthropogenic emissions. Increases
71 in emissions, such as from shipping (Gong et al., 2018) or boreal fires can affect Arctic air quality (Schmale et al.,
72 2018).

73 Ozone radiative forcing resulting from changes in tropospheric O₃ in the Arctic is highly sensitive to altitude. The
74 sensitivity of the Arctic O₃ vertical profile, and resultant forcing, from particular anthropogenic emission sources
75 and regions, vary substantially with altitude (Rap et al., 2015). Arctic surface O₃ may be most sensitive to European
76 or local sources (Sand et al., 2015; AMAP 2015; 2022), whereas emissions from North American and Asian
77 sources are more important in the mid- and upper troposphere (Monks et al., 2015; Wespes et al., 2012). Therefore,
78 a combination of varied source sensitivities in the vertical profile and the increased efficacy of longwave O₃ forcing
79 with altitude in the troposphere leads to a complex picture in terms of drivers of climate forcing by Arctic O₃. The
80 presence of temperature inversions in the Arctic lower troposphere may result in negative local forcing (Rap et al.,
81 2015; Flanner et al., 2018), in particular for local sources such as shipping (Marelle et al., 2018). Hence, to improve
82 the quantification of O₃ radiative effects in the Arctic there is a need first to assess model performance in terms of
83 seasonal cycles and vertical distributions. The annual mean vertical distributions of O₃ and CO were examined in
84 AMAP (2022) and Whaley et al. (2022) as compared to TES and MOPITT satellite retrievals. Those studies



85 showed good agreement between models and satellite measurements for O₃ in the free troposphere, where it is a
86 strong GHG.

87 This paper assesses the current state of knowledge about the dynamics of Arctic tropospheric O₃ and the ability of
88 a suite of current chemistry-transport and chemistry-climate models to simulate seasonal cycles of O₃ and selected
89 precursors. We first review our current understanding of sources and sinks of Arctic tropospheric O₃ in Section 2.
90 We summarize the models used in this study in Section 3 and the recent findings from satellite observations in
91 Section 4. We then examine the extent to which our understanding of Arctic tropospheric O₃ can explain observed
92 seasonal cycles at different surface sites in the Arctic and assess the ability of models to simulate observed
93 distributions (Section 5). We also examine vertical distributions of O₃ and its precursors and the extent to which
94 models are able to capture observed seasonal variations (Section 6). Finally, conclusions are presented in Section
95 7. Trends in Arctic tropospheric O₃ over the last 20-30 years and possible changes in seasonal cycles are presented
96 in a companion paper and compared to results from a subset of these models (Law et al., 2022).

97 **2. Arctic O₃: sources and sinks**

98 This section reviews tropospheric O₃ sources and sinks that are particularly relevant to the Arctic region, and many
99 of these processes are shown in the schematic in Figure 1.

100 **2.1 Ozone sources**

101 Tropospheric O₃ is a secondary air pollutant, which is not directly emitted but produced from the photochemical
102 reactions of anthropogenic and natural precursor emissions of VOCs, CO and CH₄ in the presence of NO_x. Besides
103 significant anthropogenic sources of these O₃ precursors, there are also important natural sources for these species,
104 such as boreal fires, lightning, vegetation and transport of O₃ from the stratosphere, which show marked seasonal
105 and inter-annual variations (Figure 1). Away from the surface, and in remote environments the tropospheric O₃
106 lifetime is around 20 days or more (Young et al., 2013), which facilitates the long-range transport of O₃ in the
107 troposphere. Production of O₃ from lower latitude emission sources and its subsequent transport to the Arctic is a
108 substantial source of Arctic tropospheric O₃, where the dry Arctic conditions and stably stratified atmosphere
109 further prolong the O₃ lifetime. In addition, the stratosphere-troposphere exchange of O₃ makes a substantial
110 contribution to the Arctic O₃ budget, where a lower tropopause height compared to the tropics facilitates the import
111 of stratospheric air masses rich in O₃. The weak in-situ O₃ formation in the Arctic relative to lower latitudes
112 increases the relative importance of this exchange. More recently, a new understanding has emerged regarding
113 contributions to Arctic surface O₃ from both anthropogenic and natural near-Arctic sources of O₃ precursors.

114 Downward transport of O₃ from the stratosphere is an important source of O₃ in the Arctic troposphere and may
115 be key in driving seasonality in Arctic tropospheric O₃ (Shapiro et al., 1987, Hess and Zbinden, 2013, Ancellet et
116 al., 2016). The Liang et al. (2009) modeling study suggests that in spring (March and April), most of the O₃ in the
117 Arctic upper troposphere originates from the stratospheric injection (78%) and that 20-25% of surface O₃
118 originates from direct injection of O₃ or the injection of NO_y and secondary O₃ formation. Analysis of observations
119 by Tarasick et al. (2019a) is consistent with this picture. Global model simulations conducted as part of the Coupled
120 Model Intercomparison Project Phase 6, suggest an increase in near-surface O₃ over the Arctic during the 21st



121 century, driven by increased stratospheric O₃ import into the troposphere, particularly in winter (Zanis et al., 2022).
122 In contrast, during summer, the dominant source of Arctic tropospheric O₃ is in-situ production in the Arctic,
123 which in July contributes more than 50% of O₃ in the Arctic boundary layer and 30-40% in the free troposphere
124 (Walker et al., 2012). This study also showed that the transport of peroxyacetyl nitrate (PAN) from lower latitudes
125 is the dominant source of NO_x, driving in-situ O₃ production at the surface in late spring and early summer.
126 Methane (CH₄) is a key precursor for tropospheric O₃, via its oxidation in the presence of sufficient NO_x.
127 Anthropogenic CH₄ emissions are estimated to be responsible for around half of the global radiative forcing due
128 to tropospheric O₃ from pre-industrial to present-day (Stevenson et al. 2013). Fiore et al. (2008) estimated that
129 anthropogenic CH₄ emissions contribute 15% to the annual average total global O₃ burden (including natural and
130 anthropogenic sources). Based on parameterised source-receptor sensitivities for a range of CMIP6 SSP scenarios,
131 Turnock et al. (2019) illustrated the significant contribution of CH₄ to future O₃ concentration reductions at high
132 latitudes. Using a similar approach, based on parameterised responses to O₃ precursor emission perturbations found
133 that CH₄ dominates the sensitivity of Arctic O₃ to anthropogenic emissions (AMAP, 2015). CH₄ accounts for
134 approximately 40% of the Arctic O₃ response to precursor emission perturbations (AMAP, 2015).

135 Import of O₃ and its precursors from lower latitudes associated with episodes of long-range transport of
136 anthropogenic or biomass burning pollution leads to enhancements in Arctic tropospheric O₃ (Wespes et al., 2012;
137 Monks et al., 2015; Ancellet et al., 2016). Whilst very low levels of NO_x within the Arctic, away from local
138 sources, often limit local O₃ production, the release of NO_x from thermal decomposition of peroxy-acetyl nitrate
139 (PAN) (an important NO_x reservoir) imported from lower latitudes, can lead to in-situ production of O₃,
140 particularly in the warmer Arctic summer lower troposphere (Wespes et al., 2012; Arnold et al., 2015).
141 Investigation of long-range transport of O₃ precursors has shown efficient export of PAN from East Asia to the
142 North Pacific, with relative contributions to long-range O₃ transport of 35% in spring and 25% in summer (Jiang
143 et al., 2016). Ship observations over the Arctic and Bering Seas also identified events of long-range pollution
144 transport with enhancements in O₃ (Kanaya et al., 2019).

145 Recently, there has been progress in improving knowledge of local O₃ precursor sources. Surface O₃ in summer is
146 already influenced by shipping NO_x emissions along the northern Norwegian coast (Marelle et al., 2016; Marelle
147 et al., 2018) and the Northwest Passage (Aliabadi et al., 2015). Marelle et al., (2018) showed for a 2050 scenario,
148 including diversion shipping in the Arctic, shipping would become the main surface O₃ source. Tuccella et al.
149 (2017) showed that background O₃ is influenced by emissions downwind of oil and gas extraction platforms in the
150 southern Norwegian Sea. Granier et al. (2006) predicted the increase in shipping activity during the summer would
151 increase O₃ levels by a factor of 2-3 in the coming decades, with maximum increases (> 20 ppbv) occurring in the
152 Canadian Archipelago, Beaufort Sea, central Arctic Ocean, and the Siberian sector of the Arctic.

153 Natural sources of Arctic tropospheric O₃ precursors include lightning NO_x, emissions of NO_x and reactive VOCs
154 from the snowpack (Honrath et al., 1999; Guimbaud et al., 2002; Hornbrook et al., 2016; Pernov et al., 2021), and
155 natural emissions of VOCs from high latitude vegetation (Holst et al., 2010; Ghirardo et al., 2020), and the Arctic
156 Ocean (Mungall et al., 2017). Evidence from both observations and models suggests that boreal fires are also an
157 important source of O₃ precursors and NO_x reservoir species like PAN, in spring and summer, with impacts on
158 Arctic O₃ (Thomas et al., 2013; Arnold et al., 2015; Viatte et al., 2015; Ancellet et al., 2016).



159 2.2 Ozone sinks

160 Photochemical loss of O₃ is mainly via photolysis in the presence of water vapor or direct reaction of O₃ with
161 hydroperoxyl or hydroxyl radicals (HO₂ or OH). Photochemical destruction involving the hydroperoxyl radical
162 (HO₂) may be particularly important in the Arctic where water vapor abundances are low (Arnold et al. 2015).
163 Where local emission sources give rise to high NO_x concentrations in urban regions or regions of shipping activity,
164 O₃ loss via titration with NO can be dominant (Thorp et al., 2021; Raut et al., 2022). Dry deposition of O₃ and its
165 precursors to ice and ocean surfaces is slower than to vegetated terrestrial surfaces (Figure 1). Van Dam et al.
166 (2016) reported O₃ dry deposition velocities that were 5 times higher over Arctic snow-free tundra in the summer
167 months at Toolik Lake (northern Alaska) compared to the snow-covered ground. Dry deposition, combined with
168 possible chemical loss (e.g. involving Biogenic-Volatile Organic Compounds, BVOCs) producing lower O₃
169 concentrations during stable (lower light) night conditions may explain the different diurnal cycle observed at this
170 tundra site compared to Arctic coastal locations. Interestingly, gradient studies at Barrow showed a positive
171 gradient with height during O₃ depletion events (ODE) and atmospheric mercury depletion events (AMDE)
172 suggesting that O₃ was removed at the surface due to fast photochemical reactions at or close to snow surfaces
173 initiated by the release of halogen species (Skov et al., 2006). During ODEs at Arctic sites in the Canadian
174 archipelago (Alert, Resolute, and Eureka), vertical profiles show ozone is typically uniformly depleted in the
175 boundary layer whereas a positive gradient is observed above the boundary layer (Tarasick and Bottenheim, et al.,
176 2002).

177 During Arctic spring, photochemical cycling of halogens in so-called ‘bromine explosion’ events leads to rapid
178 depletion of surface O₃ to low or near-zero concentrations (Barrie et al. 1988; Simpson et al. 2007). These
179 phenomena are most commonly observed at Arctic coastal locations in March/April and attributed to bromine
180 (halogen) sources linked to Arctic sea ice, coupled with stable surface temperature inversions (e.g. Figure 1;
181 Hermann et al., 2019). Interestingly, Yang et al. (2020) and Huang et al. (2020) were able to explain major
182 depletion events in a model study by introducing the wind-induced release of bromine from the snowpack.
183 However, the models could not explain the depletion events observed at low wind speeds. Swanson et al. (2022)
184 used the GEOS-Chem model to show that both blowing snow and the snowpack are important sources of bromine
185 during the spring. Figure 2 shows the vertical extent of low O₃ episodes observed by lidar at Eureka in northern
186 Canada. On May 7th, low O₃ concentrations were observed and back trajectories showed that air masses came in
187 from the ice-covered Arctic Ocean and had been in contact with the surface multiple times during the previous 6
188 days, whereas the concentrations were high on May 9, when air came down from the mountains located to the
189 south (Seabrook and Whiteway, 2016). Peterson et al. (2018) showed that active halogen chemistry and related O₃
190 depletion can also occur up to 200 km inland over snow-covered tundra in Alaska. Simpson et al. (2018) reported
191 high levels of bromine oxide (BrO) at Utqiagvik (previously known as Barrow, Alaska) occurring earlier in
192 February in air masses originating from the Arctic Ocean polar night. Their findings suggest a dark wintertime
193 source of reactive bromine (halogens) that could feed halogen photochemistry at lower latitudes as the sun returns.

194 In addition, whilst earlier studies proposed indirect evidence that O₃ and gaseous elemental mercury (Hg⁰) is
195 removed by reaction with Br atoms (e.g. Skov et al. 2004; Skov et al. 2020; Dastoor et al. 2008), Wang et al.
196 (2019) showed, for the first time, a direct connection between O₃ and Hg⁰ with atomic bromine (Br) during O₃ and
197 Hg⁰ depletion episodes at Utqiagvik, on the north coast of Alaska (see Figure 3) where O₃ and Hg⁰ are removed



198 in competing reactions with Br. Here, the Br/BrO ratio anti-correlates with O₃ concentrations and box modeling
199 confirms that O₃ is removed by Br.

200 This result is significant since the main source of halogens in the Arctic is the release from refreezing snow and
201 ice, snow blowing over sea ice, heterogeneous reactions of aerosol particles, and snowpack recycling (Petersen et
202 al. 2016; Peterson et al., 2017, Wang et al., 2017; Yang et al. 2020). Burd et al. (2017) found a strong relationship
203 between the end of the reactive bromine season and snowmelt timing. In the future, continued decreases in Arctic
204 sea ice extent or the relative distributions of multi-year/seasonal sea-ice cover, coupled with increases in the length
205 of the snow-free season over land could influence the magnitude and seasonality of O₃ sinks via changes in halogen
206 fluxes or dry deposition fluxes to tundra/ocean rather than snow/ice surfaces.

207 3. AMAP models and simulations

208 To evaluate our process understanding of controls on the Arctic tropospheric O₃ budget and distribution, we
209 evaluate a suite of model simulations. Twelve atmospheric models participated in this study; 7 chemical-transport
210 models (DEHM, EMEP-MSC W, GEOS-Chem, MATCH, MATCH-SALSA, OsloCTM, WRF-Chem) and 5
211 chemistry-climate models (CESM, CMAM, GISS-E2.1, MRI-ESM2, and UKESM1), with simulations of the years
212 2014–2015 for comparisons to observations. All models used the same set of anthropogenic emissions called
213 ECLIPSEv6b (AMAP 2022), though had different sources for fire, biogenic emissions, and meteorology (see
214 Table S1). All participating models prescribe CH₄ concentrations based on box model results, which are, in turn,
215 based on the ECLIPSEv6b anthropogenic CH₄ emissions, and various assumptions on natural CH₄ emissions
216 (Olivié et al., 2021; Prather et al., 2012). Models then allow CH₄ to take part in photochemical processes. The
217 participating models have varying degrees of spatial resolution and chemical complexity; air quality-focused
218 models, such as DEHM, EMEP MSC-W, GEOS-Chem, MATCH, and WRF-Chem have detailed HO_x-NO_x-
219 hydrocarbon O₃ chemistry, with speciated volatile organic compounds (VOCs), and secondary aerosol formation,
220 and tend to run at higher resolution. The earth system models GISS-E2.1, MRI-ESM2, and UKESM1 also contain
221 this level of tropospheric chemistry, though run globally at coarser resolution. Whereas, climate-focused models
222 like CMAM, run at a coarse resolution and have simplified tropospheric chemistry in order to be able to run for
223 long periods. For example, CMAM's tropospheric chemistry consists only of CH₄-NO_x-O₃ chemistry, with no
224 VOCs.

225 As mentioned above, Arctic tropospheric O₃ is heavily influenced by imports from the stratosphere. The models
226 vary, too, in their representation of the stratosphere. Only a subset of participating models have a fully simulated
227 stratosphere. CMAM, MRI-ESM2, GISS-E2.1, OsloCTM, and UKESM1 contain relatively complete stratospheric
228 O₃ chemistry (NO_x, NO_x, Cl_x, Br_x chemistry that controls stratospheric O₃). Other models have a simplified
229 stratosphere, such as GEOS-Chem which has a linearized stratospheric chemistry scheme (LINOZ, McLinden et
230 al., 2000), and WRF-Chem which specifies stratospheric concentrations from climatologies. Finally, several
231 models have no stratosphere or stratospheric chemistry at all (e.g., DEHM, and EMEP MSC-W). Most atmospheric
232 models, including all of the models in this study, do not yet contain Arctic tropospheric bromine chemistry, and
233 thus cannot simulate the surface-level bromine-driven O₃ depletion events that occur during spring. However,



234 there are research versions of some models which are starting to contain this chemistry (e.g., Parrella et al., 2012;
235 Falk and Sinnhuber, 2018; Badia et al., 2021)

236 These same 12 model simulations were also evaluated against a different set of measurements in AMAP (2022)
237 and Whaley et al. (2022). Those studies focused on many SLCF species over the Northern Hemisphere and
238 generally reported model biases for the annual mean concentrations. They found that all models overestimated
239 surface O₃ concentrations at mid-latitudes, but that there were both over- and underestimation in the Arctic.
240 Particularly, models overestimated surface O₃ in the western Arctic (e.g., Alaska), particularly in the summertime,
241 but were better able to simulate the surface O₃ seasonal cycle in the eastern Arctic (e.g., northern Europe). They
242 also found that model biases were small throughout the free-troposphere when compared to remote measurements
243 from the Tropospheric Emission Spectrometer (TES) satellite instrument.

244 In the next sections, these models are compared with observations of O₃ and its precursors either individually, or
245 as the multi-model median (MMM) - whereby the median of all 12 atmospheric models is shown unless otherwise
246 noted. The model output was selected from the model grid box that contains the latitude and longitude of the
247 observation location without any spatial interpolation.

248 **4. Arctic-wide tropospheric distributions from satellite data**

249 Despite the potential limitations of some satellite data products at high latitudes, several studies have exploited
250 satellite observations to investigate tropospheric O₃ and precursor distributions and trends relevant to the Arctic.
251 Pommier et al. (2012) presented IASI retrievals of 0-8 km and 0-12 km sub-column O₃ for the Arctic in spring and
252 summer 2008. These showed widespread enhancements in spring-time (Mar-Apr) tropospheric O₃ column
253 compared with summer (Jun-Jul), particularly over northeast Siberia, northern Canada and the Arctic Ocean.
254 Generally, good agreement with in-situ aircraft profiles was demonstrated, but negative IASI biases were found
255 compared with aircraft data in the lower troposphere, due to low thermal contrast in the Arctic boundary layer.
256 Wespes et al., (2012) showed that IASI was able to detect enhancements in mid-latitude sourced O₃ enhancements
257 during summer at the edge of the Arctic, but also showed a lack of sensitivity over snow and ice surfaces,
258 potentially resulting in missing some O₃ enhancements. Sodemann et al. (2011) analyzed the cross-polar transport
259 of a large pollution plume originating from Asia during the summer of 2008 using IASI CO retrievals. IASI was
260 able to detect features and structures of the plume consistent with in-situ aircraft data.

261 Satellite observations are also useful in evaluating the sources and export of O₃ precursors from mid-latitude source
262 regions and their subsequent transport to the Arctic. Tropospheric NO₂ columns measured from OMI have been
263 used to detect enhancements and trends in NO_x emissions due to gas flaring in high latitude (up to 67°N) areas of
264 Russia and North America (Li et al., 2016). Assessment of a suite of chemical transport models using OMI
265 tropospheric NO₂ columns for summer 2008 showed a potential overestimate in NO₂ over biomass burning regions
266 in eastern Siberia, with lower biases over European and North American source regions, and model under-
267 estimates over China (Emmons et al., 2015). A comparison of regional model-simulated tropospheric NO₂ columns
268 with observations from the OMI satellite instrument suggests potential underestimates in anthropogenic NO₂
269 emissions over high latitude Siberia and the Russian Arctic (Thorp et al., 2021). Monks et al., (2015) exploited
270 limited profile information from MOPITT CO retrievals to evaluate relationships between CO seasonal cycles in



271 the lower and upper troposphere over the Arctic and mid-latitude source regions. Atmospheric Infrared Sounder
272 (AIRS) CO retrievals from 2007 to 2018 have been used to characterize atmospheric circulation patterns coincident
273 with pollution enhancements during Arctic spring (Thomas et al., 2021), and IASI CO column measurements have
274 been used to analyze transport pathways for Asian anthropogenic pollution to the Arctic (Ikeda et al., 2021). Osman
275 et al. (2016) constructed three-dimensional ($5^\circ \times 5^\circ \times 1$ km) gridded climatologies of CO via a domain-filling
276 trajectory mapping technique based on MOZAIC-IAGOS in situ measurements of commercial aircraft flights.
277 These climatologies agreed well using forward and backward trajectories ($< 10\%$ difference for most cases) and
278 against vertical measurements from MOZAIC-IAGOS not included in the climatologies. These climatologies were
279 compared with CO retrievals from MOPITT, small biases were found in the lower troposphere while differences
280 of $\sim 20\%$ were found between 500 and 300 hPa, which declined throughout the study (2001-2012). Inter-annual
281 variability in PAN retrieved by TES over Eastern Siberia for April 2006-2008 was documented by Zhu et al.,
282 (2015), and it was shown to be largely controlled by boreal fire emissions at this time of year. More recently, PAN
283 data from the TES instrument was used to help characterize Asian influence on exported PAN and downwind O_3
284 production (Jiang et al., 2016). A temperature-dependent high bias in TES PAN was found at cold temperatures
285 over high latitudes.

286 In both Chapter 7 of the 2022 AMAP SLCF report (AMAP, 2022) and Whaley et al. (2022), data from satellite
287 instruments, TES, ACE-FTS, and MOPITT are used to evaluate modeled O_3 , CH_4 , and CO in the Northern
288 Hemisphere. They showed that model biases for CH_4 were small, though tended to be negative in the Arctic due
289 to a lack of north-south gradient in the prescribed global distribution. Model biases were also negative for free-
290 tropospheric O_3 , however, it was by approximately the same amount that TES O_3 retrievals have been shown to
291 be biased high by Verstraeten et al. (2013). The ACE-FTS comparison for O_3 showed good agreement but had
292 higher model biases around 300-100 hPa in Whaley et al. (2022) and AMAP (2022). The MOPITT CO
293 comparisons in AMAP (2022) showed that all models' CO are biased low over land in the mid-latitudes, but biased
294 high over the oceans at lower latitudes. Monks et al. (2015) discussed that models had high biases in the outflow
295 from Asia, and low biases north of there due to lack of transport. The Quennehen et al. (2016) study also suggested
296 that summertime CO transport out of Asia is too zonal. This could explain some of the underestimations in the
297 Arctic CO in the mid-troposphere.

298 **5. Arctic surface O_3 and precursors: seasonal cycles**

299 In the high Arctic, there is very little diurnal variation in surface O_3 , most likely because the local and regional
300 photochemistry is of limited importance most of the time and due to the 24-hour daylight during Arctic spring,
301 summer and Autumn as well as the polar night during winter, see earlier. For High Arctic sites, the seasonal
302 dynamics of O_3 can be explained mostly by long-range transport and particularly in the winter and springtime,
303 intrusion from aloft, see Figure 5a. Moving southwards to the Polar Circle a clearer diurnal pattern is evident
304 caused both by the seasonal behavior of vertical mixing, deposition, transport, and local chemistry (references) as
305 the stations on the Scandinavian peninsula, and Denali central Alaska.

306



307 **5.1 Surface Ozone**

308 Seasonal differences in the Arctic are important because of differences between the local meteorological
309 conditions, as well as atmospheric transport, in the warm and the cold seasons and seasonal variations in O₃ sources
310 and sinks. Surface O₃ at remote midlatitude sites with limited influence from local and regional anthropogenic O₃
311 precursor emissions have been found to frequently exhibit a characteristic seasonal cycle with peak values during
312 spring and a minimum in the summer, while sites with high exposure to O₃ from anthropogenic precursors have
313 summer time O₃ maxima (Monks 2000; Parrish et al. 2013, 2019; Gaudel et al., 2018). The spring maxima has
314 been explained by stratospheric intrusions as well as enhanced photochemical formation during this period of the
315 year. The summer minima, e. g. observed at the Mace Head site (Derwent et al., 1998, 2013, 2020), which is
316 strongly influenced by marine air, appears to be explained by photochemical destruction in the absence of
317 anthropogenic precursors. Seasonal cycles at Arctic stations are not extensively discussed in the literature, but it
318 is evident that the halogen chemistry discussed above, most frequently observed at high Arctic coastal stations,
319 leads to a significant reduction during the springtime (e.g. Oltman and Komhyr, 1986; Tarasick et al., 1995; Monks
320 et al., 2015). Regarding the more southerly Arctic and near-Arctic sites, a latitudinal gradient has been observed
321 in the timing of the spring O₃ maximum. Anderson et al. (2017) found that monthly mean observed near-surface
322 O₃ concentrations at background sites in Sweden from 1990 to 2013 had a maximum in spring, but the most
323 northerly stations experienced their maximum in April while the more southerly ones in May.

324 In order to get an overview of the annual O₃ cycles at different types of Arctic surface measurement sites, we have
325 calculated the monthly medians and interquartile range for the period 2003-2019 for a series of sites. A map of the
326 stations as well as their coordinates and elevation can be seen in Figure 4. Figure 5 illustrates the range of seasonal
327 cycle behavior observed in the Arctic at different measurement sites and shows different seasonal cycles depending
328 on location.

329 **5.1.1 High Arctic sites**

330 Figure 5a shows that the seasonalities in O₃ at Villum, Barrow/Utqiagvik, Alert, Tiksi and Eureka are similar:
331 They have a local minimum in spring due to the occurrence of ODEs, a slight increase/recovery in June and a
332 second minimum in July due to surface removal and photochemical degradation of O₃. These stations are located
333 at high latitude coastal sites close to sea level. During winter, O₃ reaches a maximum, due to an absence of
334 photochemical degradation of O₃, vertical mixing is suppressed during polar night since the Arctic boundary layer
335 is often highly stratified, thus hampering removal by dry deposition (Esau and Sorokina, 2016).

336 **5.1.2 Near Arctic Circle sites**

337 The characteristic seasonal variations of surface O₃ measured at stations close to the Arctic Circle are shown in
338 Figure 5b. The stations are Karasjok and Tustervatnet in Norway, Esrange in Sweden, Pallas in Finland and Denali
339 in Alaska. The sites in Figure 5b, which are not influenced by ODEs, exhibit a yearly cycle that is more similar to
340 lower latitude European stations at remote locations. Here, surface O₃ exhibits a late spring maximum which is
341 attributed to photochemical production and transport of O₃ from the stratosphere (Monks, 2000). The largest
342 differences between the stations are mainly found during the summer months, most likely due to the influence of
343 local sources on photochemical O₃ production.



344 Kårvatn in Norway has an unusual behavior with an O₃ maximum in March, possibly due to the local conditions:
345 The site often shows a pronounced diurnal cycle in O₃ due to the location at the bottom of a valley that causes
346 strong inversions leading to an enhanced impact of dry deposition at night on surface O₃ (Aas et al., 2017).

347 Hurdal in Norway is included as an example of a more southerly Scandinavian non-Arctic station, which has an
348 annual variation with a minimum in October while the more northerly stations have minima between July and
349 September (Figure 5c), this difference may be explained by a stronger influence of local air pollution at Hurdal.
350 At Hurdal, winter O₃ concentrations are particularly low, probably also in this case due to the influence of local
351 emissions which in this period leads to the removal of O₃ by the reaction with NO.

352 5.1.3 Other sites: Inland high-elevation

353 Summit (located in the free troposphere on the Greenland Ice Sheet) is much less affected by bromine chemistry
354 originating from sea ice or other low altitude processes than the coastal High Arctic sites (Huang et al. 2017).
355 Consequently, the seasonal variation is different with a clear maximum in May, a minimum in September, the
356 higher concentrations compared to other surface stations can be explained by the high sensitivity to stratospheric
357 O₃ enriched air (Monks et al., 2015) at this high elevation (3211 masl) site. Short episodes of depletion have been
358 reported (Brooks et al. 2011) but they do not appear to affect the monthly mean values substantially as shown in
359 Figure 5c.

360 Zeppelin, although a high Arctic site, is located on a mountain ridge at 474 masl and thus experiences free
361 tropospheric air masses more often compared to sea level sites. For this reason, it is less influenced by ODEs and
362 consequently does not have an O₃ minimum in spring like the other high Arctic coastal stations (Figure 5c). That
363 said, the occasional ODE has been reported there by Lehrer et al. (1997) and Ianniello et al. (2021).

364 We also note that surface O₃ can be influenced by local anthropogenic emissions such as shipping (e.g. Marelle et
365 al., 2016, Aliabadi et al., 2015) or oil field emissions (McNamara et al., 2019). McNamara et al. (2019) discussed
366 potentially important interactions between local anthropogenic NO_x emissions from the Barrow settlement or the
367 Prudhoe Bay oil extraction facilities in northern Alaska and snowpack (chlorine) chemistry leading to elevated
368 concentrations of nitrogen-containing compounds (e.g. N₂O₅, HO₂NO₂), with implications for Arctic tropospheric
369 O₃. Therefore, while none of the Arctic sites currently exhibit summertime surface maxima due to photochemical
370 production, as often observed in polluted locations further south, this may change in the future with increasing
371 local anthropogenic emissions (e.g. Marelle et al. 2018).

372 He et al. (2016) measured O₃ and black carbon on a ship cruise to the Arctic Ocean (31.1°N to 87.7°N and 9.3°E–
373 90°E to 168.4°W) from June to September 2012. Comparing the observed O₃ concentrations to those measured at
374 Barrow showed no statistically significant differences, the authors suggest that coastal stations between July and
375 September may be representative of the entire Arctic but this hypothesis requires further investigation. Indeed, our
376 results show significant differences in the O₃ seasonal cycles at different Arctic locations depending on whether
377 they were coastal, in-land, or high elevation.

378



379 5.2 Surface O₃ model evaluation

380 It has been found that halogen chemistry, stable boundary layers, and dry deposition explained differences between
381 measured and modeled O₃ concentrations, as demonstrated by Kanaya et al. (2019) who performed measurements
382 of CO and O₃ during several ship cruises in the Bering Sea and the Arctic Ocean in September (2012 to 2017).
383 None of the models in our study contain surface halogen chemistry but they also display highly variable agreement
384 in their surface O₃ seasonal cycles. Figure 6 shows the seasonal cycle from the models and observations averaged
385 for 2014-15 at several Arctic observation locations. Since the models do not contain surface-level bromine
386 chemistry, at locations like Alert and Barrow/Utqiagvik, they do not capture the springtime minimum in O₃. Some
387 models (e.g. UKESM1) greatly underestimate wintertime O₃. This may be related to deficiencies in boundary layer
388 mixing or an overly shallow boundary layer depth, resulting in the overly active titration of O₃ by NO near NO_x
389 emission sources and subsequent underestimation of Arctic surface O₃. However, other model deficiencies could
390 also play a role, including dry deposition and NO_x lifetime. Indeed, Barten et al. (2021) found that overestimation
391 of oceanic O₃ deposition can explain some differences between modeled and measured surface O₃ in the High
392 Arctic. Some models in Figure 6 do not agree on the timing of the springtime peak, with CMAM, DEHM, and
393 GISS-E2.1 peaking in April, and EMEP-MSC-W and MRI-ESM2 peaking in May/June. The same groupings of
394 models display different O₃ behavior at the end of the year (October-December), with CMAM, DEHM, and GISS-
395 E2.1 all correctly simulating an increase in O₃, and EMEP-MSC-W and MRI-ESM2 having a decrease. All models
396 agree better with observations and each other on summertime surface O₃ abundance at all locations, and on the
397 full seasonal cycle at Summit, the high-elevation background location. The large range of modeled surface O₃ is
398 similar to previous model studies (Shindell et al., 2008; Monks et al., 2015; Gaudel et al., 2018). Despite the large
399 range in model performance, the overall average negative O₃ bias, and the seasonality in model bias at
400 Barrow/Utqiagvik and Summit, are consistent with these previous studies. The comparisons highlight little change
401 in the skill of models in simulating Arctic surface O₃ over the past decade.

402 These particular model simulations have been evaluated in Whaley et al. (2022), where they grouped all western
403 Arctic (defined as lat > 60°N, and lon < 0°) and eastern Arctic (lat > 60°N, lon > 0°) O₃ measurements together, and
404 showed the range in modeled and measured seasonal cycles for those two regions. That analysis included
405 additional locations at lower latitudes, thus their results emphasized that some models overestimated summertime
406 O₃ in the western Arctic. Otherwise, the results from that study are consistent with what we report here.

407 5.3 Ozone precursors

408 NO_x monitors have been used at several Arctic sites but in a study at Zeppelin, it was shown that most of the NO_x
409 was in the form of the NO_x reservoir species PAN (Beine et al., 1997; Beine and Krognnes, 2000). We evaluate and
410 discuss PAN in Section 6.3 from aircraft measurements. There are only limited sources for NO_x in the Arctic and
411 the lifetime of NO_x is in the order of a day. Whaley et al. (2022) evaluated surface NO_x volume mixing ratios and
412 found that these models underestimated surface NO₂ by -59% at low-Arctic latitudes that were mostly around
413 60°N.

414 The dominant source for NO_x is long-range transport of dominantly PAN (Beine and Krognnes; 2000), and
415 particulate bound HNO₃ followed by reactivation in the Arctic by thermal decomposition and photoreduction



416 processes, respectively. Kramer et al. (2015) determined at Summit from July 2008 to July 2010 that PAN
417 accounted for 295 ppt, and NO_x for 88 ppt. In a more recent study, Huang et al. (2017) found in the period July
418 2008–June 2010, PAN and NO_x were maximum in spring at about 250 ppt and 25 ppt, respectively, and in summer
419 75 ppt and 20 ppt, respectively. Beine and Krognes, (2000) measured PAN at Zeppelin Mountain between 1994
420 and 1996. They found median values were lowest in summer at 89.4 ppt and highest in spring at 222.6 ppt. HNO₃
421 in the gas phase is in general very low (Wespes et al., 2012). Particulate bound nitrate – potentially a significant
422 source of NO_x in the atmosphere and snow pack – is close to the detection limit in summer and up to 124.7 ng N
423 m⁻³ in winter e.g. at Villum (Nguyen et 2013).

424 In general, NMVOC concentrations in the Arctic are low and thus their photo-oxidation has only a limited impact
425 on O₃. There is a series of studies dedicated to specific source regions and emission sources. There is one long
426 term measurement study by Gautrois et al. (2003); studies focusing on long-range transport (Stohl, 2006; Harrigan
427 et al., 2011), snowpack emissions (Boudries et al., 2002; Dibb and Arsenault, 2002; Guimbaud et al., 2002; Barret
428 et al., 2011; Gao et al., 2012) and shipborne measurements (Sjostedt et al., 2012 and Mungall et al., 2017). The
429 Gautrois et al. (2003) study reported long-term VOC concentrations for Alert, NU, they found yearly levels of
430 ethane, propane and toluene are 1.7 ppbv, 0.6 ppbv and 26 pptv, respectively. For comparison, mixing ratios of
431 ethane, propane, and toluene in China ranged from 3.7-17 ppbv, 1.5-20.8 ppbv, 0.4-11.2 ppbv, respectively
432 (Barletta et al., 2005).

433 Pernov et al. (2021) measured organic O₃ precursors online with a PTR-ToF-MS at Villum from April to October
434 2018. Sources were apportioned with Positive Matrix Factorization During the late spring, the Arctic haze factor
435 was a source of oxygenated VOCs (OVOCs) arising from long-range transport of anthropogenic emissions whilst
436 during summer OVOCs and DMS originated from the Marine cryosphere factor. During autumn, the Biomass
437 burning factor peaked in importance and was dominated by acetonitrile. The most abundant compound during the
438 campaign was acetone with a mean mixing ratio of 0.6 ppbv, for benzene 0.027 ppbv and DMS 0.046 ppbv. In the
439 future, local NMVOC emissions might increase from both natural and anthropogenic sources due to the retreating
440 sea ice with more biological activity and more industrial activity and shipping affecting future levels of O₃.

441 Figure 7 shows the observed and simulated seasonal cycle of CO at Zeppelin and Utqiagvik/Barrow. Simulated
442 CO ranges about 50 ppbv across models, and all models underestimate surface CO at these sites. The low model
443 biases are dominated by the winter and spring months. The 2014-15 annual multi-model median (MMM) bias is -
444 11% and -16% at Zeppelin and Barrow/Utqiagvik, respectively. Figure 7 shows that for the first 6 months of the
445 year, the MMM is 20-30% too low, but that in the summer, the MMM is much closer to observations. These CO
446 results are very similar to those found in previous multi-model studies (Shindell et al., 2008; Monks et al., 2015;
447 Whaley et al., 2022). Similar to O₃, these results imply little change in the skill of models in simulating Arctic
448 surface CO over the past decade. The modeled CO underestimations are well-reported in the literature, and
449 attributed either to a lack of CO from combustion sources in the emission inventories (e.g., Kasibhatla et al., 2002;
450 Pétron et al., 2002; Jiang et al., 2015), or to errors in OH, which impact the lifetime of CO (e.g., Monks et al.,
451 2015; Quennehen et al., 2016). Indeed both may be at cause here, as the anthropogenic CO emissions from
452 ECLIPSEv6b are lower than those in the CMIP6 emission inventory, neither of which have taken into account the
453 reported discrepancies from top-down emissions studies (Kasibhatla et al., 2002; Pétron et al., 2002; Jiang et al.,



454 2015, Miyazaki et al., 2020). Monks et al. (2015) showed that models with lower global mean OH concentrations
455 produced smaller underestimates in Arctic surface CO and that models with larger underestimates in CO over mid-
456 latitude source regions also had larger underestimates in Arctic CO. Emmons et al. (2015) showed that the models
457 with larger tropospheric OH also had higher photolysis rates of O₃ to O^{1D} and that there was also some relationship
458 between higher photolysis rates and lower cloud cover fraction in some models. Previous multi-model results have
459 also shown that variability in model water vapour abundance in the Arctic appeared to be the leading driver of
460 model variability in OH, despite being much less important at lower latitudes (Monks et al., 2015). Evaluating OH
461 and water vapour is unfortunately beyond the scope of our study.

462 Methane has more than doubled since preindustrial times (from 0.8 ppmv to 1.8 ppmv) and the photooxidation of
463 methane in the presence of NO_x is a source of O₃. Thawing permafrost and release from organic deposits in shallow
464 Arctic Ocean waters in a warmer climate presents a new source of methane (Isaksen et al. 2014). The models of
465 this study prescribed CH₄ concentrations, including their increasing trend, and they were found to have a small
466 bias of ~2% in Whaley et al. (2022) compared to surface and satellite measurements. Going forward, models are
467 starting to simulate CH₄ explicitly from emissions, and this will be important for simulating future changes in
468 Arctic tropospheric chemistry.

469 6. Vertical distributions of O₃ and precursors in the Arctic

470 Observations and models have both demonstrated extensive layering of pollution signatures in the Arctic
471 troposphere vertical profile, associated with varying air mass origins with altitude (Zheng et al., 2021; Willis et
472 al., 2019). Large-scale isentropic transport pathways result in air masses from warmer more southerly latitudes
473 being imported into the Arctic upper troposphere, while emissions from cooler northerly latitudes enter the Arctic
474 near the surface and in the lower troposphere (Stohl, 2006). The presence of the Arctic dome during winter
475 essentially shuts off access to the Arctic surface to air mass import from southerly mid-latitudes, while it facilitates
476 efficient low-level transport of emissions from Northern Eurasia and Russia to the Arctic surface, giving rise to
477 the well-known Arctic haze (Shaw, 19995). In practice, this large-scale dynamical control on long-range transport
478 to the Arctic gives rise to a well-characterized vertical dependence of source region sensitivities for O₃ and
479 precursors through the Arctic troposphere, where emissions from South and East Asia have the most influence in
480 the Arctic upper troposphere, emissions from North America have the most influence in the Arctic mid-
481 troposphere, and northern Eurasian and Russian emissions dominate at the surface (in addition to local influences)
482 (Wespes et al., 2012; Monks et al., 2015). As mentioned in Section 1, this vertical layering and changes in the
483 efficacy of O₃ radiative forcing with altitude has implications for the sensitivity of Arctic tropospheric O₃ forcing
484 to regional emission perturbations.

485 Despite evidence for extensive vertical layering in the Arctic troposphere, and the potential for highly varying
486 source contributions with altitude, aside from a limited set of regular O₃ sonde profiles, there is a severe lack of
487 observations available on the vertical distribution of O₃, and particularly its precursors, in the Arctic troposphere.
488 There is an especially poor constraint on seasonal and interannual variability in O₃ precursor profiles. In this
489 section, we make use of available vertical profile measurements of O₃ and its precursors to document our
490 understanding of Arctic tropospheric O₃ profiles, and to evaluate model-simulated vertical profiles of O₃ and
491 precursors.



492 6.1 Ozonesondes

493 Ozone soundings provide a long-term record of Arctic O₃ through the depth of the troposphere. Since 1966, weekly
494 soundings have been available at Resolute and since the 1980s regular soundings, typically once a week, have
495 been available from 6 stations north of 60°N (Figure 4, Table S.2). All of these stations are located in the sector
496 95°W to 27°E meaning that regular soundings are lacking in a large sector of the Arctic. The measurements are
497 conducted using the balloon-borne Electrochemical Concentration Cell (ECC) ozonesondes, typically reaching an
498 altitude of about 30 km. Random uncertainties in tropospheric measurements are about 5%, and biases reported
499 from field and laboratory comparisons to UV reference photometers are 1.0±4.4% in the lower troposphere and
500 5.3±4.4% in the upper troposphere (Tarasick et al., 2019b). Mean observed concentrations have a minimum close
501 to the surface and then gradually increase throughout the troposphere by about 50% and then increase sharply
502 going into the upper troposphere and lower stratosphere (Figure 8 and Figure S.1-2). Observed seasonal cycles in
503 the Arctic troposphere generally show a maximum in spring and summer and a minimum in fall and winter (Paper
504 2).

505 Christiansen et al. (2017) examined long-term ozonesonde records at 9 Arctic stations reporting consistent seasonal
506 cycles as a function of altitude between sites with later maxima in the mid-troposphere compared to the surface
507 layers and upper troposphere.

508 6.2 Model evaluation against ozonesondes

509 Figure 8 shows a comparison of the ozonesonde measurements at Eureka to the simulations from the 12
510 participating models for the annual and seasonal averages for the years 2014-15. In the supplement (Figure S.2),
511 model-measurement comparisons at other Arctic locations are shown. Generally, the models are highly variable,
512 ranging +/-50% of the measured O₃ profiles at most seasons and locations. However, the MMM performs well and
513 is within +/-8% throughout most of the troposphere. However, all models, except UKESM1, have a bulge with a
514 high model bias around 300-400 hPa, which is at or near the tropopause, implying that most models simulate the
515 tropopause height too low (having larger stratospheric O₃ concentrations appearing too low in altitude). This results
516 in a positive bias of about 20% for the MMM around the tropopause. This feature in models was also reported in
517 AMAP (2015), where model biases were particularly large at Ny Alesund and Summit. They associated those with
518 differences in the transport of air masses from the stratosphere. This issue will have an impact on estimating the
519 tropospheric O₃ burden, which is a common climate diagnostic (e.g., Griffiths et al., 2021).

520 At Alert, there are both surface and ozonesonde measurements, and we find that the results in the lowest levels of
521 the Alert ozonesonde comparisons (Figure S.1) are consistent with the model biases found in Figure 8 in that both
522 show the models underestimating winter and fall O₃, overestimating spring, and matching well with observations
523 in the summer at this location.

524 Note that the models' monthly average O₃ values were used in this comparison, which does not match the time of
525 day and day of the week as the ozonesonde measurements. However, when a careful time-matching to 3-hourly
526 model output is carried out, the general features of the model biases remain the same (Figure S.2), likely because
527 of the lack of a strong diurnal cycle in Arctic O₃ and its relatively long lifetime in the free troposphere.



528 The results of this model evaluation of the Arctic O₃ vertical profiles are consistent with Whaley et al. (2022),
529 which compared the same model simulations to TES O₃ retrievals throughout the troposphere at lower Arctic
530 locations (~60-70 °N). They found models to be biased low (around -10%), though the TES measurements have
531 been shown to be biased high by about the same amount (+13% bias in TES measurements reported in Verstraeten
532 et al., (2013)). They also saw a small positive shift in the model bias profile around 300 hPa as well. Finally, the
533 Whaley et al. (2022) study included O₃, NO_x, CH₄, and CO comparisons to the Atmosphere Chemistry Experiment
534 (ACE)-Fourier Transform Spectrometer (FTS) satellite instrument, and those results also implied, independently,
535 that the modeled tropopause heights are too low.

536 **6.3 Vertical distribution of O₃ precursors**

537 Intensive field measurement campaigns using aircraft provide the most detailed observational constraint on vertical
538 profiles of tropospheric O₃ precursors in the Arctic. While these datasets tend to provide excellent spatial and
539 temporal resolution measurements on a wide range of species, they are episodic in nature, often covering only a
540 period of a few days to several weeks, flying in specific regions of the Arctic and often targeting specific layers or
541 plumes. For example, Ancellet et al. (2016) examined aircraft, lidar and ozonesonde data over Canada and
542 Greenland during the summer of 2008 POLARCAT campaigns (Law et al., 2014). This study showed clear
543 latitudinal and longitudinal variations in the origins of sampled air masses based on back trajectories and O₃-
544 potential vorticity (PV) correlations. While downward transport of O₃ was important over Greenland, air masses
545 with higher O₃ were attributed to North American boreal fires over Canada. Transport of polluted air masses from
546 mid-latitudes also contributed, for example from Asia north of 80 °N.

547 The airborne NASA Atom (Atmospheric Tomography) mission (Wofsy et al., 2018) has undertaken extensive
548 surveying of the global troposphere. This includes repeated vertical profile measurements between 60 °N and 90
549 °N providing useful insights into the variation of O₃ and its precursors through the depth of the Arctic troposphere
550 at different times of the year. Figure 9 shows these mean results and their standard deviation on the left-side panels,
551 while the equivalent MMM results are on the right-side panels. The models' monthly mean results went into the
552 MMM calculation and the standard deviation from the models is shown.

553 The results show that near-surface NO₂ is greatly enhanced during winter, associated with a longer NO₂ lifetime
554 and accumulation of pollution in the Arctic haze. The MMM simulates the surface NO₂ increase and the seasonality
555 of the NO₂ profiles reasonably well. However, generally, the modeled NO₂ is biased low in the tropospheric profile,
556 having average values of about 15 pptv in the 2-6 km range, whereas the measurements are about 25 pptv on
557 average. This underestimate is consistent with that found at the surface in Whaley et al. (2022). PAN is also
558 enhanced at the surface in the winter and can thermally decompose in the spring and summer to release NO_x. The
559 MMM generally overestimates PAN (Figure 9c-d) and does not simulate the same shape in vertical profiles. For
560 example, models are not able to simulate the wintertime surface level increase in PAN, and they have the inverse
561 shape in April/May than the observed profile. The best agreement is in summertime PAN (July-Aug), when the
562 MMM vertical profile better matches that of the observations. The underestimate of NO_x and the lack of winter
563 surface increases in PAN by the models may be a reason why the wintertime surface O₃ concentrations in Section
564 5.2 and Figure 5 were underestimated. That said, it is possible that the NO_x measurements are biased high and the
565 PAN measurements are biased low due to thermal degradation in the sample line.



566 In line with ozonesonde data and previous airborne campaigns (AMAP, 2015), ATom profiles also demonstrate a
567 springtime enhancement in O_3 extending through the troposphere, with evidence of stratospheric influence in the
568 upper troposphere and lower O_3 in the summertime lower troposphere. The models capture that springtime O_3
569 enhancement as well. Summer enhancements in O_3 precursors, such as CO and PAN in the mid-troposphere, were
570 also observed associated with the import of forest fire and anthropogenic emissions from lower latitudes, as also
571 seen during POLARCAT in 2008. The models capture this feature for PAN, but less so for CO. Indeed, most
572 models underestimate CO. The annual mean, MMM bias for surface CO in the northern hemisphere has been
573 reported to be -30% (Whaley et al., 2022). Figure 9 shows that below the tropopause, modeled O_3 is actually close
574 to observed O_3 , despite the significant MMM biases for CO, NO_x , and PAN. Around the tropopause, the aircraft
575 data show the same issue that the ozonesonde data did – that models overestimate O_3 significantly near the
576 tropopause.

577 7. Conclusions

578 Recent research on Arctic tropospheric O_3 has resulted in improvements to our understanding of this pollutant and
579 GHG in the rapidly changing and sensitive Arctic environment. We have shown in this study that Arctic surface
580 O_3 seasonal cycles are different depending on whether sites are near the coast, inland, or at high elevation. Coastal
581 sites have springtime minima due to halogen chemistry causing ODEs and show a maximum during the winter.
582 The inland, near-Arctic circle locations have quite consistent seasonal cycles, with maxima in April and minima
583 in August. While the high-elevation sites, less influenced by halogen chemistry than coastal locations, are more
584 variable; Summit has a later maximum (May), and minimum (September), while Zeppelin has an earlier maximum
585 (March) and minimum (July).

586 Despite model development that has occurred since the 2015 AMAP assessment report on ozone (AMAP, 2015)
587 to add processes, improve parameterizations, increase resolution, etc, the resulting performance of the models
588 remains more or less the same in terms of model variability and biases compared to measured O_3 and O_3 -precursor
589 species in the Arctic. Model results for CO would improve if CO emissions from combustion were increased, as
590 suggested in the literature. It would also be useful to compare modeled OH in the Arctic, but that was beyond the
591 scope of this study. However, as Arctic O_3 is limited by NO_x availability, improvements to CO may not have a
592 large effect on O_3 . Improvements to modeled PAN and NO_x are needed, however, sensitivity studies to determine
593 the cause of the model biases will be required to improve model performance for those species. For surface O_3
594 distributions in the Arctic, models simulate background levels reasonably well (e.g., at the high-elevation location
595 of Summit), but surface bromine/halogen chemistry needs to be included to simulate springtime surface O_3 at
596 coastal Arctic locations (e.g., Villum, Alert, and Utqiagvik). Except near the tropopause, models simulate O_3
597 throughout the vertical profile well, with the MMM performing best at +/- 8% depending on the location and
598 altitude in the troposphere. Attention to improving the height of the modeled tropopause and/or the stratosphere-
599 tropospheric exchange is still required since downward transport of high stratospheric O_3 concentrations is causing
600 model biases around 6 to 8 km (400 to 300 hPa) to be significantly large (>20%).

601 While they are logistically challenging, additional O_3 measurements in the Arctic, such as O_3 deposition
602 measurements, observations of stratospheric-tropospheric exchange, and O_3 concentrations in the Siberian Arctic,
603 together with long-term measurements of O_3 precursors, would be particularly helpful to improve our



604 understanding and modeling capabilities. This is particularly important as climate change alters the chemistry and
605 dynamics of tropospheric O₃ in the future.

606 **Author contributions**

607 CHW, KSL, JLH, HS, SRA, JL, and JBP wrote the manuscript and created Figures 3-9. RYC, JF, and XD provided
608 the GEOS-Chem model output. JF, ST, and DT edited and provided comments on the manuscript. JHC provided
609 the DEHM model output. GF, UI, and KT provided the GISS-E2.1 model output. MG and ST provided the EMEP-
610 MSCW model output. KSL, JCR, TO, and LM provided the WRF-Chem model output. MD and NO provided the
611 MRI-ESM2 model output. DAP provided the CMAM model output. LP provided the CESM model output. RS
612 provided the OsloCTM model output. MAT provided the MATCH-SALSA model output. SRA and STT provided
613 the UKESM1 model output. DT provided the Canadian ozonesonde measurements, and DW provided Alert
614 datasets. MF and KvS provided the model strategy for this project.

615 **Competing interests**

616 At least one of the (co-)authors is a member of the editorial board of Atmospheric Chemistry and Physics. The
617 peer-review process was guided by an independent editor, and the authors also have no other competing interests
618 to declare.

619 **Special issue statement**

620 This article is part of the special issue “Arctic climate, air quality, and health impacts from short-lived climate
621 forcers (SLCFs): contributions from the AMAP Expert Group (ACP/BG inter-journal SI)”. It is not associated
622 with a conference.

623 **Acknowledgements**

624 We wish to acknowledge Wang and Pratt for their figure originally published in PNAS, as well as Seabrooke and
625 Whiteway for their figure originally published in JGR. We thank Garance Bergeron for providing the processed
626 ATOM observations. The technicians and logistical support staff at the different stations are gratefully
627 acknowledged for their work.

628 **Financial support**

629 Makoto Deushi and Naga Oshima were supported by the Japan Society for the Promotion of Science KAKENHI
630 (grant numbers: JP18H03363, JP18H05292, JP19K12312, JP20K04070 and JP21H03582), the Environment
631 Research and Technology Development Fund (JPMEERF20202003 and JPMEERF20205001) of the
632 Environmental Restoration and Conservation Agency of Japan, the Arctic Challenge for Sustainability II (ArCS
633 II), Program Grant Number JPMXD1420318865, and a grant for the Global Environmental Research Coordination
634 System from the Ministry of the Environment, Japan (MLIT1753 and MLIT2253). Joakim Langner and Manu A.
635 Thomas were supported by the Swedish Environmental Protection Agency through contracts NV-03174-20 and
636 the Swedish Clean Air and Climate research program. Svetlana Tsyro and Michael Gauss have received support
637 from the AMAP Secretariat and the EMEP Trust Fund. Ulas Im received support from the Aarhus University
638 Interdisciplinary Centre for Climate Change (iClimate) OH fund (no. 2020-0162731), the FREYA project funded
639 by the Nordic Council of Ministers (grant agreement nos. MST-227-00036 and MFVM-2019-13476), and the
640 EVAM-SLCF funded by the Danish Environmental Agency (grant agreement no. MST-112-00298). Henrik Skov
641 received funding from the Danish Ministry for Energy, Climate and Utilities (Grant agreement no. 2018-3767)
642 and Danish Environmental Agency (grant agreement no. MST-113-00140) and AMA. Kostas Tsigaridis and



643 Gregory Faluvegi received support from the NASA Modeling, Analysis and Prediction Program (MAP). Steven
644 T Turnock would also like to acknowledge the financial support received from the Arctic Monitoring and
645 Assessment Programme. Kathy S. Law, Jean-Christophe Raut, Louis Marelle and Tatsuo Onishi (LATMOS)
646 acknowledge support from EU iCUPE (Integrating and Comprehensive Understanding on Polar Environments)
647 project (grant agreement n°689443), under the European Network for Observing our Changing Planet (ERA-
648 Planet), and from access to IDRIS HPC resources (GENCI allocation A009017141) and the IPSL mesoscale
649 computing center (CICLAD: Calcul Intensif pour le CLimat, l'Atmosphère et la Dynamique) for model
650 simulations. Jesper Christensen (DEHM model) acknowledges Danish Environmental Protection Agency and
651 Danish Energy Agency (DANCEA funds for Environmental Support to the Arctic Region project: grant no. 2019-
652 7975, grant no. MST-112- 00298, grant no. TAS 4005-0153). Stephen R. Arnold and Steven T. Turnock both
653 acknowledge the financial support received from the Arctic Monitoring and Assessment Programme. Stephen R.
654 Arnold also acknowledges support from the UK Natural Environment Research Council and Belmont Forum via
655 the ACROBEAR project (grant NE/T013672/1). Joshua Fu received funding from the Oak Ridge Leadership
656 Computing Facility at the Oak Ridge National Laboratory, which is supported by the Office of Science of the U.S.
657 Department of Energy under Contract No. DE-AC05-00OR22725.

658 References

- 659 Aas, W., Fiebig, M., Solberg, S., & Yttri, K. E.: Monitoring of long-range transported air pollutants in Norway,
660 annual Report 2016 (Miljødirektoratet rapport, M-780/2017) (NILU report, 18/2017). Kjeller: NILU., 2017.
- 661 Abbatt, J. P. D., Thomas, J. L., Abrahamsson, K., Boxe, C., Granfors, A., Jones, A. E., King, M. D., Saiz-Lopez,
662 A., Shepson, P. B., Sodeau, J., Toohey, D. W., Toubin, C., von Glasow, R., Wren, S. N., and Yang, X.:
663 Halogen activation via interactions with environmental ice and snow in the polar lower troposphere and other
664 regions, *Atmos. Chem. Phys.*, 12, 6237–6271, <https://doi.org/10.5194/acp-12-6237-2012>, 2012.
- 665 Aliabadi, A.A., Staebler, R., Sangeeta, S.: Air quality monitoring in communities of the Canadian Arctic during
666 the high shipping season with a focus on local and marine pollution. *Atmospheric Chemistry and Physics*. 15,
667 2651–2673. 10.5194/acp-15-2651-2015, 2015.
- 668 Aliabadi, A. A., Thomas, J. L., Herber, A. B., Staebler, R. M., Leaitch, W. R., Schulz, H., Law, K. S., Marelle,
669 L., Burkart, J., Willis, M. D., Bozem, H., Hoor, P. M., Köllner, F., Schneider, J., Levasseur, M., and Abbatt,
670 J. P. D.: Ship emissions measurement in the Arctic by plume intercepts of the Canadian Coast Guard
671 icebreaker Amundsen from the Polar 6 aircraft platform, *Atmos. Chem. Phys.*, 16, 7899–7916,
672 <https://doi.org/10.5194/acp-16-7899-2016>, 2016.
- 673 AMAP: Arctic Monitoring and Assessment Programme, Assessment 2022: short-lived climate forcers, Technical
674 report, AMAP, Oslo, Norway, <https://www.amap.no/> (last access: 14 April 2022), in press, 2022.
- 675 AMAP: Arctic Monitoring and Assessment Programme, Assessment 2015: Black carbon and ozone as Arctic
676 climate forcers, Technical report, AMAP, Oslo, Norway, vii C 116 pp.,
677 [https://www.amap.no/documents/doc/amap-assessment-2015-black-carbon-and-ozone-as-arctic-climate-](https://www.amap.no/documents/doc/amap-assessment-2015-black-carbon-and-ozone-as-arctic-climate-forcers/1299)
678 [forcers/1299](https://www.amap.no/documents/doc/amap-assessment-2015-black-carbon-and-ozone-as-arctic-climate-forcers/1299) (last access: 14 April 2022), 2015.
- 679 Ancellet, G., Daskalakis, N., Raut, J. C., Tarasick, D., Hair, J., Quennehen, B., Ravetta, F., Schlager, H.,
680 Weinheimer, A. J., Thompson, A. M., Johnson, B., Thomas, J. L., and Law, K. S.: Analysis of the latitudinal
681 variability of tropospheric ozone in the Arctic using the large number of aircraft and ozonesonde
682 observations in early summer 2008, *Atmos. Chem. Phys.*, 16, 13341–13358, [https://doi.org/10.5194/acp-16-](https://doi.org/10.5194/acp-16-13341-2016)
683 [13341-2016](https://doi.org/10.5194/acp-16-13341-2016), 2016.



- 684 Andersson, C., Alpfjord, H., Robertson, L., Karlsson, P. E., and Engardt, M.: Reanalysis of and attribution to
685 near-surface ozone concentrations in Sweden during 1990–2013, *Atmos. Chem. Phys.*, 17, 13869–13890,
686 <https://doi.org/10.5194/acp-17-13869-2017>, 2017.
- 687 Arnold, S. R., Emmons, L. K., Monks, S. A., Law, K. S., Ridley, D. A., Turquety, S., Tilmes, S., Thomas, J. L.,
688 Bouarar, I., Flemming, J., Huijnen, V., Mao, J., Duncan, B. N., Steenrod, S., Yoshida, Y., Langner, J., and
689 Long, Y.: Biomass burning influence on high-latitude tropospheric ozone and reactive nitrogen in summer
690 2008: a multi-model analysis based on POLMIP simulations, *Atmos. Chem. Phys.*, 15, 6047–6068,
691 [doi:10.5194/acp-15-6047-2015](https://doi.org/10.5194/acp-15-6047-2015), 2015.
- 692 Badia, A., Iglesias-Suarez, F., Fernandez, R. P., Cuevas, C. A., Kinnison, D. E., Lamarque, J.-F., et al.: The role
693 of natural halogens in global tropospheric ozone chemistry and budget under different 21st century climate
694 scenarios, *Journal of Geophysical Research: Atmospheres*, 126, e2021JD034859,
695 <https://doi.org/10.1029/2021JD034859>, 2021.
- 696 Bahramvash Shams, S., Walden, V. P., Petropavlovskikh, I., Tarasick, D., Kivi, R., Oltmans, S., Johnson, B.,
697 Cullis, P., Sterling, C. W., Thölix, L., and Errera, Q.: Variations in the vertical profile of ozone at four high-
698 latitude Arctic sites from 2005 to 2017, *Atmos. Chem. Phys.*, 19, 9733–9751, <https://doi.org/10.5194/acp-19-9733-2019>, 2019.
- 700 Barrie, L., Bottenheim, J., Schnell, R., Crutzen, P. J., Rasmussen, R. A.: Ozone destruction and photochemical
701 reactions at polar sunrise in the lower Arctic atmosphere. *Nature* 334, 138–141,
702 <https://doi.org/10.1038/334138a0>, 1988.
- 703 Barletta, B., Meinardi, S., Sherwood Rowland, F., Chan, C.-Y., Wang, X., Zou, S., Yin Chan, L., and Blake, D.
704 R.: Volatile organic compounds in 43 Chinese cities, *Atmospheric Environment*, 39, 5979–5990,
705 <https://doi.org/10.1016/j.atmosenv.2005.06.029>, 2005.
- 706 Barten, J. G. M., L. N. Ganzeveld, G.-J. Steeneveld, M. C. Krol: Role of oceanic deposition in explaining
707 temporal variability in surface ozone at High Arctic sites, *Atmos. Chem. Phys.*, 21, 10229–10248,
708 <https://doi.org/10.5194/acp-21-10229-2021>, 2021.
- 709 Beine, H. J., Jaffe, D. a., Herring, J. a., Kelley, J. a., Krognnes, T., and Stordal, F.: High-Latitude Springtime
710 Photochemistry. Part I: NO_x, PAN and Ozone Relationships, *Journal of Atmospheric Chemistry*, 27, 127–
711 153, <https://doi.org/10.1023/A:1005869900567>, 1997.
- 712 Beine, H. J. and Krognnes, T.: The seasonal cycle of peroxyacetyl nitrate (PAN) in the European Arctic,
713 *Atmospheric Environment* 34, 933–940, 2000.
- 714 Brooks, S., C. Moore, D. Lew, B. Lefer, G. Huey, and D. Tanner: Temperature and sunlight controls of mercury
715 oxidation and deposition atop the Greenland ice sheet, *Atmospheric Chemistry and Physics* 11(16): 8295–
716 8306, 2011.
- 717 Burd, J. A., P. K. Peterson, S. V. Nghiem, D. K. Perovich, and W. R. Simpson: Snowmelt onset hinders bromine
718 monoxide heterogeneous recycling in the Arctic, *J. Geophys. Res. Atmos.*, 122, 8297–8309,
719 [doi:10.1002/2017JD026906](https://doi.org/10.1002/2017JD026906), 2017.
- 720 Christiansen, B., Jepsen, N., Kivi, R., Hansen, G., Larsen, N., and Korsholm, U. S.: Trends and annual cycles in
721 soundings of Arctic tropospheric ozone, *Atmos. Chem. Phys.*, 17, 9347–9364, <https://doi.org/10.5194/acp-17-9347-2017>, 2017.
- 723 Emmons, L. K., Arnold, S. R., Monks, S. A., Huijnen, V., Tilmes, S., Law, K. S., Thomas, J. L., Raut, J.-C.,
724 Bouarar, I., Turquety, S., Long, Y., Duncan, B., Steenrod, S., Strode, S., Flemming, J., Mao, J., Langner, J.,
725 Thompson, A. M., Tarasick, D., Apel, E. C., Blake, D. R., Cohen, R. C., Dibb, J., Diskin, G. S., Fried, A.,
726 Hall, S. R., Huey, L. G., Weinheimer, A. J., Wisthaler, A., Mikoviny, T., Nowak, J., Peischl, J., Roberts, J.
727 M., Ryerson, T., Warneke, C., and Helmig, D.: The POLARCAT Model Intercomparison Project (POLMIP):
728 overview and evaluation with observations, *Atmos. Chem. Phys.*, 15, 6721–6744, [doi:10.5194/acp-15-6721-2015](https://doi.org/10.5194/acp-15-6721-2015), 2015.



- 730 Dastoor, A. P., Davignon, D., Theys, N., Van Roozendael, M., Steffen, A., and Ariya, P. A.: Modeling Dynamic
731 Exchange of Gaseous Elemental Mercury at Polar Sunrise, *Environ. Sci. Technol.*, 42, 5183–5188, 2008.
- 732 Esau, I. and S. Sorokina: Climatology of the Arctic Planetary Boundary Layer, Chapter 1 in *Atmospheric*
733 *Turbulence, Meteorological Modeling*, ISBN 978-1-60741-091-1, Eds: Peter R. Lang and Frank S.
734 Lombargo, 2016.
- 735 Falk, S. and B.-M. Sinnhuber: Polar boundary layer bromine explosion and ozone depletion events in the
736 chemistry–climate model EMAC v2.52: implementation and evaluation of AirSnow algorithm, *Geosci.*
737 *Model Dev.*, 11, 1115–1131, <https://doi.org/10.5194/gmd-11-1115-2018>, 2018.
- 738 Fiore, A. M., J. J. West, L. W. Horowitz, V. Naik, and M. D. Schwarzkopf: Characterizing the tropospheric
739 ozone response to methane emission controls and the benefits to climate and air quality, *J. Geophys. Res.*,
740 113, D08307, doi:10.1029/2007JD009162, 2008.
- 741 Flanner, M. G., Huang, X., Chen, X., and Krinner, G.: Climate Response to Negative Greenhouse Gas
742 Radiative Forcing in Polar Winter, *Geophysical Research Letters*, 45, 1997–2004,
743 <https://doi.org/10.1002/2017GL076668>, 2018.
- 744 Gaudel, A., A. Gaudel, O. R. Cooper, G. Ancellet, B. Barret, A. Boynard, J. P. Burrows, C. Clerbaux, P.-F.
745 Coheur, J. Cuesta, E. Cuevas, S. Doniki, G. Dufour, F. Ebojic, G. Foret, O. Garcia, M. J. Granados-Muñoz, J.
746 W. Hannigan, F. Hase, B. Hassler, G. Huang, D. Hurtmans, D. Jaffe, N. Jones, P. Kalabokas, B. Kerridge, S.
747 Kulawik, B. Latter, T. Leblanc, E. Le Flochmoën, W. Lin, J. Liu, X. Liu, E. Mahieu, A. McClure-Begley, J.
748 L. Neu, M. Osman, M. Palm, H. Petetin, I. Petropavlovskikh, R. Querel, N. Rapp, A. Rozanov, M. G.
749 Schultz, J. Schwab, R. Siddans, D. Smale, M. Steinbacher, H. Tanimoto, D. W. Tarasick, V. Thouret, A. M.
750 Thompson, T. Trickl, E. Weatherhead, C. Wespes, H. M. Worden, C. Vigouroux, X. Xu, G. Zeng, J. Ziemke:
751 Tropospheric Ozone Assessment Report: Present-day distribution and trends of tropospheric ozone relevant
752 to climate and global atmospheric chemistry model evaluation. *Elem Sci Anth*, 6, 39, doi:
753 <https://www.elementscience.org/articles/10.1525/elementa.291>, 2018.
- 754 Gautrois, M., Brauers, T., Koppmann, R., Rohrer, F., Stein, O., and Rudolph, J.: Seasonal variability and trends
755 of volatile organic compounds in the lower polar troposphere, *J. Geophys. Res.*, 108, 4393,
756 doi:10.1029/2002JD002765, D13, 2003.
- 757 Ghirardo A, Lindstein F, Koch K, et al.: Origin of volatile organic compound emissions from subarctic tundra
758 under global warming. *Glob Change Biol*. 26:1908–1925. <https://doi.org/10.1111/gcb.14935>, 2020.
- 759 Gong, W., Beagley, S. R., Cousineau, S., Sassi, M., Munoz-Alpizar, R., Ménard, S., Racine, J., Zhang, J., Chen,
760 J., Morrison, H., Sharma, S., Huang, L., Bellavance, P., Ly, J., Izdebski, P., Lyons, L., and Holt, R.:
761 Assessing the impact of shipping emissions on air pollution in the Canadian Arctic and northern regions:
762 current and future modeled scenarios, *Atmos. Chem. Phys.*, 18, 16653–16687, <https://doi.org/10.5194/acp-18-16653-2018>, 2018.
- 764 Guimbaud, C., A. M. Grannas, P. B. Shepson, J. D. Fuentes, H. Boudries, J. W. Bottenheim, F. Dominé, S.
765 Houdier, S. Perrier, T. B. Biesenthal, B. G. Splawn: Snowpack processing of acetaldehyde and acetone in the
766 Arctic atmospheric boundary layer, *Atmos. Environ.*, 36, 2743–2752, doi:10.1016/S1352-2310(02)00107-
767 3, 2002.
- 768 Granier, C., Niemeier, U., Jungclaus, J. H., Emmons, L., Hess, P., Lamarque, J.-F., Walters, S., and Brasseur, G.
769 P.: Ozone pollution from future ship traffic in the Arctic northern passages, *Geophysical Research Letters*,
770 33, <https://doi.org/10.1029/2006GL026180>, 2006.
- 771 Griffiths, P. T., Murray, L. T., Zeng, G., Shin, Y. M., Abraham, N. L., Archibald, A. T., Deushi, M., Emmons, L.
772 K., Galbally, I. E., Hassler, B., Horowitz, L. W., Keeble, J., Liu, J., Moeini, O., Naik, V., O'Connor, F. M.,
773 Oshima, N., Tarasick, D., Tilmes, S., Turnock, S. T., Wild, O., Young, P. J., and Zanis, P.: Tropospheric
774 ozone in CMIP6 simulations, *Atmos. Chem. Phys.*, 21, 4187–4218, [https://doi.org/10.5194/acp-21-4187-](https://doi.org/10.5194/acp-21-4187-2021)
775 2021, 2021.



- 776 Harrigan, D. L., Fuelberg, H. E., Simpson, I. J., Blake, D. R., Carmichael, G. R., and Diskin, G. S.:
777 Anthropogenic emissions during Arctas-A: mean transport characteristics and regional case studies, *Atmos.*
778 *Chem. Phys.*, 11, 8677–8701, <https://doi.org/10.5194/acp-11-8677-2011>, 2011.
- 779 He, P., Bian, L., Zheng, X., Yu, J., Sun, C., Ye, P., and Xie, Z.: Observation of surface ozone in the marine
780 boundary layer along a cruise through the Arctic Ocean: From offshore to remote, *Atmospheric Research*,
781 *Part A* 169, pp. 191–198, doi: 10.1016/j.atmosres.2015.10.009, 2016.
- 782 Helmig, D., Petrenko, V., Martinerie, P., Witrant, E., Röckmann, T., Zuiderweg, A., Holzinger, R., Hueber, J.,
783 Thompson, C., White, J. W. C., Sturges, W., Baker, A., Blunier, T., Etheridge, D., Rubino, M., and Tans, P.:
784 Reconstruction of Northern Hemisphere 1950–2010 atmospheric non-methane hydrocarbons, *Atmos. Chem.*
785 *Phys.*, 14, 1463–1483, <https://doi.org/10.5194/acp-14-1463-2014>, 2014.
- 786 Herrmann, M., L. Cao, H. Sihler, U. Platt, and E. Guthel: On the contribution of chemical oscillations to ozone
787 depletion events in the polar spring, *Atmos. Chem. Phys.*, 19, 10161–10190, [https://doi.org/10.5194/acp-19-](https://doi.org/10.5194/acp-19-10161-2019)
788 [10161-2019](https://doi.org/10.5194/acp-19-10161-2019), 2019.
- 789 Hess, P. G. and Zbinden, R.: Stratospheric impact on tropospheric ozone variability and trends: 1990–2009,
790 *Atmos. Chem. Phys.*, 13, 649–674, doi:10.5194/acp-13-649-2013, 2013.
- 791 Hirdman, D., Sodemann, H., Eckhardt, S., Burkhart, J. F., Jefferson, A., Mefford, T., Quinn, P. K., Sharma, S.,
792 Ström, J., and Stohl, A.: Source identification of short-lived air pollutants in the Arctic using statistical
793 analysis of measurement data and particle dispersion model output, *Atmos. Chem. Phys.*, 10, 669–693,
794 <https://doi.org/10.5194/acp-10-669-2010>, 2010.
- 795 Holst, T., Arneth, A., Hayward, S., Ekberg, A., Mastepanov, M., Jackowicz-Korczynski, M., Friberg, T., Crill,
796 P. M., and Bäckstrand, K.: BVOC ecosystem flux measurements at a high latitude wetland site, *Atmos.*
797 *Chem. Phys.*, 10, 1617–1634, <https://doi.org/10.5194/acp-10-1617-2010>, 2010.
- 798 Honrath, R. E., Peterson, M. C., Guo, S., Dibb, J. E., Shepson, P. B., and Campbell, B.: Evidence of NO_x
799 production within or upon ice particles in the Greenland snowpack, *Geophys. Res. Lett.*, 26, 695–698,
800 doi:10.1029/1999GL900077, 1999.
- 801 Hornbrook, R. S., et al.: Arctic springtime observations of volatile organic compounds during the OASIS-2009
802 campaign, *J. Geophys. Res. Atmos.*, 121, 9789–9813, doi:10.1002/2015JD024360, 2016.
- 803 Huang, Y., Wu, S., Kramer, L. J., Helmig, D., and Honrath, R. E.: Surface ozone and its precursors at Summit,
804 Greenland: comparison between observations and model simulations, *Atmos. Chem. Phys.*, 17, 14661–
805 14674, <https://doi.org/10.5194/acp-17-14661-2017>, 2017.
- 806 Huang, J. J., L.; Chen, Q.; Alexander, B.; Sherwen, T.; Evans, M.; Theys, N. and Sungyeon Choi:
807 Evaluating the impact of blowing-snow sea salt aerosol on springtime BrO and O₃ in the Arctic, *Atmos.*
808 *Chem. Phys.* 20, 7335–7358, 2020.
- 809 Ianniello, A., Salzano, R., Salvatori, R., Esposito, G., Spataro, F., Montagnoli, M., Mabilia, R., and Pasini, A.:
810 Nitrogen Oxides (NO_x) in the Arctic Troposphere at Ny-Ålesund (Svalbard Islands): Effects of
811 Anthropogenic Pollution Sources, 12, 901, <https://doi.org/10.3390/atmos12070901>, 2021.
- 812 Ikeda, K., Tanimoto, H., Sugita, T., Akiyoshi, H., Clerbaux, C., Coheur, P.-F.: Model and satellite analysis of
813 transport of Asian anthropogenic pollution to the Arctic: Siberian and Pacific pathways and their
814 meteorological controls. *Journal of Geophysical Research: Atmospheres*, 126, e2020JD033459.
815 <https://doi.org/10.1029/2020JD033459>, 2021.
- 816 IPCC: Climate Change 2021: The Physical Science Basis. Contribution of Working Group I to the Sixth
817 Assessment Report of the Intergovernmental Panel on Climate Change, edited by: Masson-Delmotte, V.,
818 Zhai, P., Pirani, A., Connors, S. L., Péan, C., Berger, S., Caud, N., Chen, Y., Goldfarb, L., Gomis, M. I.,
819 Huang, M., Leitzell, K., Lonnoy, E., Matthews, J. B. R., Maycock, T. K., Waterfield, T., Yelekçi, O., Yu, R.,
820 and Zhou, B., Tech. rep., Cambridge University Press, <https://www.ipcc.ch/report/ar6/wg1/#FullReport> (last
821 access: 14 April 2022), 2021.



- 822 Isaksen, I. S. A., T. K. Berntsen, S. B. Dalsoren, K. Eleftheratos, Y. Orsolini, B. Rognerud, F. Stordal, O. A.
823 Sovde, C. Zerefos and C. D. Holmes: Atmospheric Ozone and Methane in a Changing Climate, *Atmosphere*
824 5(3): 518-535, 2014.
- 825 Kanaya, Y., Miyazaki, K., Taketani, F., Miyakawa, T., Takashima, H., Komazaki, Y., Pan, X., Kato, S.,
826 Sudo, K., Sekiya, T., Inoue, J., Sato, K., and Oshima, K.: Ozone and carbon monoxide
827 observations over open oceans on R/V Mirai from 67° S to 75° N during 2012 to 2017: testing
828 global chemical reanalysis in terms of Arctic processes, low ozone levels at low latitudes, and
829 pollution transport, *Atmos. Chem. Phys.*, 19, 7233–7254, [https://doi.org/10.5194/acp-19-7233-](https://doi.org/10.5194/acp-19-7233-2019)
830 2019, 2019.
- 831 Jiang, Z., J. R. Worden, V. H. Payne, L. Zhu, E. Fischer, T. Walker, and D. B. A. Jones: Ozone export from East
832 Asia: The role of PAN, *J. Geophys. Res. Atmos.*, 121, 6555–6563, doi:10.1002/2016JD024952, 2016.
- 833 Jiang, Z., D. B. A. Jones, J. Worden, H. M. Worden, D. K. Henze, and Y. X. Wang: Regional data assimilation
834 of multi-spectral MOPITT observations of CO over North America, *Atmos. Chem. Phys.*, 15, 6801–6814,
835 doi:10.5194/acp-15-6801-2015, 2015.
- 836 Kasibhatla, P., A. Arellano, J. A. Logan, P. I. Palmer, P. Novelli: Top-down estimate of a large source of
837 atmospheric carbon monoxide associated with fuel combustion in Asia, *Geophys. Res. Lett.*, 29(19), 1900,
838 doi:10.1029/2002GL015581, 2002.
- 839 Klimont, Z., Kupiainen, K., Heyes, C., Purohit, P., Cofala, J., Rafaj, P., Borcken-Kleefeld, J., and Schöpp, W.:
840 Global anthropogenic emissions of particulate matter including black carbon, *Atmos. Chem. Phys.*, 17, 8681–
841 8723, <https://doi.org/10.5194/acp-17-8681-2017>, 2017.
- 842 Law, K. S., J. Liengard Hjorth, J. Boyd Pernov, M. Collaud Coen, H. Langner, H. Skov, S. R. Arnold, C. H.
843 Whaley, J. Christensen, G. Faluvegi, M. Gauss, U. Im, N. Oshima, D. Plummer, K. Tsigaridis, S. Tsyro, S. T.
844 Turnock, D. Worthy: Arctic tropospheric ozone trends, *Geophys. Res. Lett.*, in preparation, 2022.
- 845 Lawrence and Mao: Anthropogenic and Natural Factors Affecting Trends in Atmospheric Methane in Barrow,
846 Alaska, *Atmosphere*, 10, 187; doi:10.3390/atmos10040187, 2019.
- 847 Lehrer, E., Wagenbach, D., & Platt, U.: Aerosol chemical composition during tropospheric ozone depletion at
848 Ny Ålesund/Svalbard, *Tellus B: Chemical and Physical Meteorology*, 49:5, 486-495, doi:
849 10.3402/tellusb.v49i5.15987, 1997.
- 850 Li, C., Hsu, N., Sayer, A., Krotkov, N., Fu, J., Lamsal, L. N., Lee, J., Tsay, S.-C.: Satellite observation of
851 pollutant emissions from gas flaring activities near the Arctic. *Atmospheric Environment* 133: 1–11.
852 doi:10.1016/j.atmosenv.2016.03.019, 2016.
- 853 Liang, Q., A. R. Douglass, B. N. Duncan, R. S. Stolarski and J. C. Witte: The governing processes and
854 timescales of stratosphere-to-troposphere transport and its contribution to ozone in the Arctic troposphere.
855 *Atmospheric Chemistry and Physics* 9(9): 3011-3025, 2009.
- 856 Lorenzen-Schmidt, H., S. Wessel, W. Unold, S. Solberg, H. Gernandt, F. Stordal and U. Platt: Ozone
857 measurements in the European Arctic during the ARCTOC 1995 campaign, *Tellus Series B-Chemical and*
858 *Physical Meteorology* 50(5): 416-429, 1998.
- 859 Mackie, A.R., P.I. Palmer, J.M. Barlow, D.P. Finch, P. Novelli and L. Jaeglé: Reduced Arctic air pollution due
860 to decreasing European and North American emissions, *J. Geophys. Res. Atmos.*, 121, 8692-8700,
861 doi:10.1002/2016JD024923, 2016.
- 862 Marelle, L., Thomas, J. L., Raut, J.-C., Law, K. S., Jalkanen, J.-P., Johansson, L., Roiger, A., Schlager, H., Kim,
863 J., Reiter, A., and Weinzierl, B.: Air quality and radiative impacts of Arctic shipping emissions in the



- 864 summertime in northern Norway: from the local to the regional scale, *Atmos. Chem. Phys.*, 16, 2359–2379,
865 <https://doi.org/10.5194/acp-16-2359-2016>, 2016.
- 866 Marelle, L., Raut, J.-C., Law, K., & Duclaux, O.: Current and future arctic aerosols and ozone from remote
867 emissions and emerging local sources—Modeled source contributions and radiative effects. *Journal of*
868 *Geophysical Research: Atmospheres*, 12 SEP 123, 12,942–12,963. <https://doi.org/10.1029/2018JD028863>, 2018.
- 869 Marelle, L., Thomas, J. L., Ahmed, S., Tuite, K., Stutz, J., Dommergue, A., Simpson, W. R., Frey, M. M., and
870 Baladima, F.: Implementation and impacts of surface and blowing snow sources of Arctic bromine activation
871 within WRF-Chem 4.1.1, *J. Adv. Model. Earth Sy.*, 13, e2020MS002391,
872 <https://doi.org/10.1029/2020MS002391>, 2021.
- 873 McNamara, S. M., A. R. W. Raso, S. Y. Wang, S. Thanekar, E. J. Boone, K. R. Kolesar, P. K. Peterson, W. R.
874 Simpson, J. D. Fuentes, P. B. Shepson and K. A. Pratt: Springtime Nitrogen Oxide-Influenced Chlorine
875 Chemistry in the Coastal Arctic, *Environmental Science & Technology* 53(14): 8057-8067, 2019.
- 876 Monks, P.: A review of the observations and origins of the spring ozone maximum, *Atmospheric Environment*,
877 34, 2000.
- 878 Monks, S. A., Arnold, S. R., Emmons, L. K., Law, K. S., Turquety, S., Duncan, B. N., Flemming, J., Huijnen,
879 V., Tilmes, S., Langner, J., Mao, J., Long, Y., Thomas, J. L., Steenrod, S. D., Raut, J. C., Wilson, C.,
880 Chipperfield, M. P., Diskin, G. S., Weinheimer, A., Schlager, H., and Ancellet, G.: Multi-model study of
881 chemical and physical controls on transport of anthropogenic and biomass burning pollution to the Arctic,
882 *Atmos. Chem. Phys.*, 15, 3575-3603, doi:10.5194/acp-15-3575-2015, 2015.
- 883 Mungall, E., Abbatt, J., Wentzell, J., Lee, A., Thomas, J., Blais, M., Gosselin, M., Miller, L., Papakyriakou, T.,
884 Willis, M. Liggio, J.: Microlayer source of oxygenated volatile organic compounds in the summertime
885 marine Arctic boundary layer. *Proceedings of the National Academy of Sciences*. 114. 201620571.
886 10.1073/pnas.1620571114, 2017.
- 887 Miyazaki, K., K. W. Bowman, K. Yumimoto, T. Walker and K. Sudo: Evaluation of a multi-model, multi-
888 constituent assimilation framework for tropospheric chemical reanalysis, *Atmos. Chem. Phys.*, 20, 931–967,
889 <https://doi.org/10.5194/acp-20-931-2020>, 2020.
- 890 Olivié, D., Höglund-Isaksson, L., Klimont, Z., and von Salzen, K.: Boxmodel for calculation of global
891 atmospheric methane concentration, Zenodo, <https://doi.org/10.5281/zenodo.5293940>, 2021.
- 892 Oltmans, S. J., and Komhyr, W. D.: Surface ozone distributions and variations from 1973–1984: Measurements
893 at the NOAA Geophysical Monitoring for Climatic Change Baseline Observatories, *J. Geophys. Res.*, 91,
894 D4, 5229– 5236, doi:[10.1029/JD091iD04p05229](https://doi.org/10.1029/JD091iD04p05229), 1986.
- 895 Osman, M. K., Tarasick, D. W., Liu, J., Moeini, O., Thouret, V., Fioletov, V. E., Parrington, M., and Nédélec,
896 P.: Carbon monoxide climatology derived from the trajectory mapping of global MOZAIC-IAGOS data,
897 *Atmos. Chem. Phys.*, 16, 10263–10282, <https://doi.org/10.5194/acp-16-10263-2016>, 2016.
- 898 Parrella, J. P., Jacob, D. J., Liang, Q., Zhang, Y., Mickley, L. J., Miller, B., Evans, M. J., Yang, X., Pyle, J. A.,
899 Theys, N., and Van Roozendaal, M.: Tropospheric bromine chemistry: implications for present and pre-
900 industrial ozone and mercury, *Atmos. Chem. Phys.*, 12, 6723–6740, [https://doi.org/10.5194/acp-12-6723-](https://doi.org/10.5194/acp-12-6723-2012)
901 2012, 2012.
- 902 Pernov, J. B., Bossi, R., Lebourgeois, T., Nøjgaard, J. K., Holzinger, R., Hjorth, J. L., and Skov, H.:
903 Atmospheric VOC measurements at a High Arctic site: characteristics and source apportionment, *Atmos.*
904 *Chem. Phys.*, 21, 2895–2916, <https://doi.org/10.5194/acp-21-2895-2021>, 2021.
- 905 Peterson, P.K., Pratt, K.A., Simpson, W.R., Nghiem, S.V., Pérez Pérez, L.X., Boone, E.J., Pöhler, D., Zielcke, J.,
906 General, S., Shepson, P.B., Frieß, U., Platt, U. and Stirm, B.H.: The role of open lead interactions in
907 atmospheric ozone variability between Arctic coastal and inland sites. *Elem Sci Anth*, 4, p.000109. DOI:
908 <http://doi.org/10.12952/journal.elementa.000109>, 2016.



- 909 Peterson, P. K., Pöhler, D., Sihler, H., Zielcke, J., General, S., Frieß, U., Platt, U., Simpson, W. R., Nghiem, S.
910 V., Shepson, P. B., Stirm, B. H., Dhaniyala, S., Wagner, T., Caulton, D. R., Fuentes, J. D., and Pratt, K. A.:
911 Observations of bromine monoxide transport in the Arctic sustained on aerosol particles, *Atmos. Chem.*
912 *Phys.*, 17, 7567–7579, <https://doi.org/10.5194/acp-17-7567-2017>, 2017.
- 913 Peterson, P.K., D. Pöhler, J. Zielcke, S. General, U. Frieß, U. Platt, W.R. Simpson, S.V. Nghiem, P.B. Shepson,
914 B.H. Stirm and K.A. Pratt: Springtime Bromine Activation over Coastal and Inland Arctic Snowpacks *ACS*
915 *Earth Space Chem*, 2, 1075–1086, DOI: 10.1021/acsearthspacechem.8b00083, 2018.
- 916 Peterson, P. K., Hartwig, M., May, N.W. , Schwartz, E., Rigor, I., Ermold, W., Steele, M., Morison, J. H.,
917 Nghiem, S. V. and Pratt, K. A.: Snowpack measurements suggest role for multi-year sea ice regions in
918 Arctic atmospheric bromine and chlorine chemistry. *Elem Sci Anth*, 7: 14,
919 doi:<https://doi.org/10.1525/elementa.352>, 2019.
- 920 Pétron, G., C. Granier, B. Khattatov, J.-F. Lamarque, V. Yudin, J.-F. Muller, J. Gille: Inverse modeling of
921 carbon monoxide surface emissions using Climate Monitoring and Diagnostics Laboratory network
922 observations, *J. Geophys. Res.-Atmospheres*, 107, D24, doi:10.1029/2001JD001305, 2002.
- 923 Pittman, J. V., L. L. Pan, J. C. Wei, F. W. Irion, X. Liu, E. S. Maddy, C. D. Barnet, K. Chance, and R.-S. Gao:
924 Evaluation of AIRS, IASI, and OMI ozone profile retrievals in the extratropical tropopause region using in
925 situ aircraft measurements, *J. Geophys. Res.*, 114, D24109, doi:10.1029/2009JD012493, 2009.
- 926 Pommier, M., Clerbaux, C., Law, K. S., Ancellet, G., Bernath, P., Coheur, P.-F., Hadji-Lazaro, J., Hurtmans, D.,
927 Nédélec, P., Paris, J.-D., Ravetta, F., Ryerson, T. B., Schlager, H., and Weinheimer, A. J.: Analysis of IASI
928 tropospheric O₃ data over the Arctic during POLARCAT campaigns in 2008, *Atmos. Chem. Phys.*, 12, 7371–
929 7389, <https://doi.org/10.5194/acp-12-7371-2012>, 2012.
- 930 Pope, R. J., Richards, N. A. D., Chipperfield, M. P., Moore, D. P., Monks, S. A., Arnold, S. R., Glatthor, N.,
931 Kiefer, M., Breider, T. J., Harrison, J. J., Remedios, J. J., Warneke, C., Roberts, J. M., Diskin, G. S., Huey, L.
932 G., Wisthaler, A., Apel, E. C., Bernath, P. F., and Feng, W.: Intercomparison and evaluation of satellite
933 peroxyacetyl nitrate observations in the upper troposphere-lower stratosphere, *Atmos. Chem. Phys.*, 16,
934 13541–13559, doi:10.5194/acp-16-13541-2016, 2016.
- 935 Prather, M. J., Holmes, C. D., and Hsu, J.: Reactive greenhouse gas scenarios: Systematic exploration of
936 uncertainties and the role of atmospheric chemistry, *Geophys. Res. Lett.*, 39, L09803,
937 <https://doi.org/10.1029/2012GL051440>, 2012.
- 938 Salmi, T., Määttä, A., Anttila, P., Ruoho-Airola, T., and Amnell, T.: Detecting trends of annual values of
939 atmospheric pollutants by the Mann-Kendall test and Sen's slope estimates – the Excel template application
940 Makesens, Finnish Meteorological Institute, Helsinki, Finland, 2002.
- 941 Raut, J.-C., K. S. Law, T. Onishi, N. Daskalakis, L. Marelle: Impact of shipping emissions on air pollution and
942 pollutant deposition over the Barents Sea, *Environmental Pollution*, 298, 118832,
943 doi:<https://doi.org/10.1016/j.envpol.2022.118832>, 2022.
- 944 Seabrook, J., and J. Whiteway: Influence of mountains on Arctic tropospheric ozone, *J. Geophys. Res. Atmos.*,
945 121, 1935–1942, doi:10.1002/2015JD024114, 2016.
- 946 Sharma, S., L. A. Barrie, E. Magnusson, G. Brattstrom, W. R. Leaitch, A. Steffen and S. Landsberger: A Factor
947 and Trends Analysis of Multidecadal Lower Tropospheric Observations of Arctic Aerosol Composition,
948 Black Carbon, Ozone, and Mercury at Alert, Canada, *Journal of Geophysical Research-Atmospheres*,
949 124(24): 14133-14161, 2019.
- 950 Shapiro, M. A., T.Hampel, and A. J. Krueger: The Arctic tropopause fold, *Mon. Wea. Rev.*, 115, 444–454,
951 doi:<https://doi.org/10.1175/1520-0493>, 1987.
- 952 Shaw, G. E.: The Arctic Haze Phenomenon, 76, 2403–2414, [https://doi.org/10.1175/1520-](https://doi.org/10.1175/1520-0477(1995)076<2403:Tahp>2.0.Co;2)
953 [0477\(1995\)076<2403:Tahp>2.0.Co;2](https://doi.org/10.1175/1520-0477(1995)076<2403:Tahp>2.0.Co;2), 1995.



- 954 Shindell, D.: Local and remote contributions to Arctic warming, *Geophys. Res. Lett.*, 34, L14704,
955 doi:10.1029/2007GL030221, 2007.
- 956 Shindell, D. T., Chin, M., Dentener, F., Doherty, R. M., Faluvegi, G., Fiore, A. M., Hess, P., Koch, D. M.,
957 MacKenzie, I. A., Sanderson, M. G., Schultz, M. G., Schulz, M., Stevenson, D. S., Teich, H., Textor, C.,
958 Wild, O., Bergmann, D. J., Bey, I., Bian, H., Cuvelier, C., Duncan, B. N., Folberth, G., Horowitz, L. W.,
959 Jonson, J., Kaminski, J. W., Marmor, E., Park, R., Pringle, K. J., Schroeder, S., Szopa, S., Takemura, T.,
960 Zeng, G., Keating, T. J., and Zuber, A.: A multi-model assessment of pollution transport to the Arctic,
961 *Atmos. Chem. Phys.*, 8, 5353–5372, <https://doi.org/10.5194/acp-8-5353-2008>, 2008.
- 962 Simpson, W. R., Frieß, U., Thomas, J. L., Lampel, J., and Platt, U.: Polar nighttime chemistry produces intense
963 reactive bromine events. *Geophysical Research Letters*, 45, 9987–9994. [https://](https://doi.org/10.1029/2018GL079444)
964 doi.org/10.1029/2018GL079444, 2018.
- 965 Simpson, W. R., von Glasow, R., Riedel, K., Anderson, P., Ariya, P., Bottenheim, J., Burrows, J., Carpenter, L.
966 J., Frieß, U., Goodsite, M. E., Heard, D., Hutterli, M., Jacobi, H.-W., Kaleschke, L., Neff, B., Plane, J., Platt,
967 U., Richter, A., Roscoe, H., Sander, R., Shepson, P., Sodeau, J., Steffen, A., Wagner, T., and Wolff, E.:
968 Halogens and their role in polar boundary-layer ozone depletion, *Atmos. Chem. Phys.*, 7, 4375–4418,
969 <https://doi.org/10.5194/acp-7-4375-2007>, 2007.
- 970 Skov, H. Brooks, S. Goodsite, M.E. Lindberg, S.E. Meyers, T.P. Landis, M.S. Larsen, M.R.B. Jensen, B.
971 McConville, G. Christensen, J.: Measuring reactive gaseous mercury flux by relaxed eddy accumulation.
972 *Atmos. Environ.* 40, 5452-5463, 2006.
- 973 Skov, H. Egeløv, A.H. Granby, K. and Nielsen, T.: The Relation of ozone with other Photochemical Products at
974 Ll. Valby, Denmark, *Atmos. Environ.*, 31, 5, 685-691, 1997.
- 975 Skov, H., J. Hjorth, C. Nordstrøm, J. B., C. C., P. M.B., L. J.B. and M. Dall’Osto: The variability in Gaseous
976 Elemental Mercury at Villum Research Station, Station Nord in North Greenland from 1999 to 2017,
977 *Atmospheric Chemistry and Physics*, 20, 13253-13265, doi:10.5194/acp-20-13253-2020, 2020.
- 978 Sodemann, H., Pommier, M., Arnold, S. R., Monks, S. A., Stebel, K., Burkhardt, J. F., Hair, J. W., Diskin, G. S.,
979 Clerbaux, C., Coheur, P.-F., Hurtmans, D., Schlager, H., Blechschmidt, A.-M., Kristjánsson, J. E., and Stohl,
980 A.: Episodes of cross-polar transport in the Arctic troposphere during July 2008 as seen from models,
981 satellite, and aircraft observations, *Atmos. Chem. Phys.*, 11, 3631–3651, [https://doi.org/10.5194/acp-11-](https://doi.org/10.5194/acp-11-3631-2011)
982 [3631-2011](https://doi.org/10.5194/acp-11-3631-2011), 2011.
- 983 Stohl, A.: Characteristics of atmospheric transport into the Arctic troposphere, *J. Geophys. Res.*, 111, D11306,
984 doi:10.1029/2005JD006888, 2006.
- 985 Swanson, W. F., Holmes, C. D., Simpson, W. R., Confer, K., Marelle, L., Thomas, J. L., Jaeglé, L., Alexander,
986 B., Zhai, S., Chen, Q., Wang, X., and Sherwen, T.: Comparison of model and ground observations finds
987 snowpack and blowing snow both contribute to Arctic tropospheric reactive bromine, *Atmos. Chem. Phys.*
988 *Discuss.* [preprint], <https://doi.org/10.5194/acp-2022-44>, in review, 2022.
- 989 Tarasick, D. W., D. I. Wardle, J. B. Kerr, J. J. Bellfleur, J. Davies: Tropospheric ozone trends over Canada: 1980-
990 1993, *Geophys. Res. Lett.*, 22, 4, 409-412, 1995.
- 991 Tarasick, D. W. and Bottenheim, J. W.: Surface ozone depletion episodes in the Arctic and Antarctic from
992 historical ozonesonde records, *Atmos. Chem. Phys.*, 2, 197–205, <https://doi.org/10.5194/acp-2-197-2002>,
993 2002.
- 994 Tarasick, D.W., T.K. Carey-Smith, W.K. Hocking, O. Moeini, H. He, J. Liu, M. Osman, A.M. Thompson, B.
995 Johnson, S.J. Oltmans and J.T. Merrill: Quantifying stratosphere-troposphere transport of ozone using
996 balloon-borne ozonesondes, radar windprofilers and trajectory models, *Atmos. Environ.*, 198 (2019), 496–
997 509, <https://doi.org/10.1016/j.atmosenv.2018.10.040>, 2019a.
- 998 Tarasick, D., Galbally, I. E., Cooper, O. R., Schultz, M. G., Ancellet, G., Leblanc, T., Wallington, T. J., Ziemke,
999 J., Liu, X., Steinbacher, M., Staehelin, J., Vigouroux, C., Hannigan, J.W., García, O., Foret, G., Zanis, P.,
1000 Weatherhead, E., Petropavlovskikh, I., Worden, H., Osman, M., Liu, J., Chang, K.-L., Gaudel, A., Lin, M.,



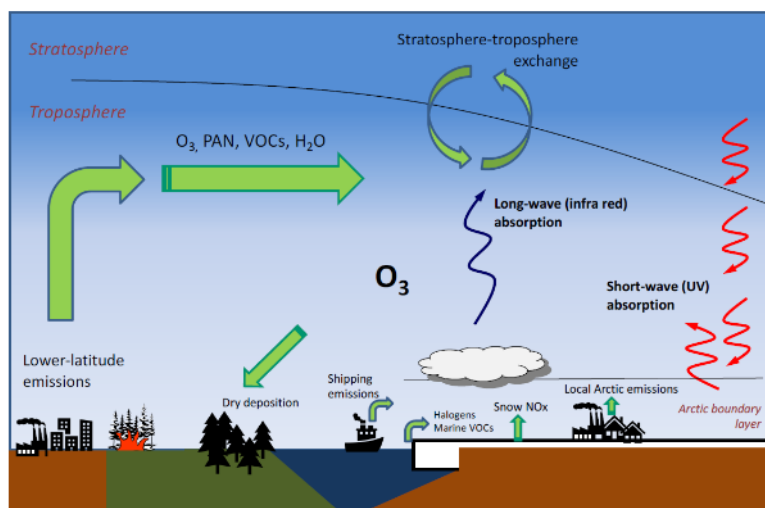
- 1001 Granados-Muñoz, M., Thompson, A. M., Oltmans, S.J., Cuesta, J., Dufour, G., Thouret, V., Hassler, B.,
1002 Trickl, T. and Neu, J.L.: Tropospheric Ozone Assessment Report: Tropospheric ozone from 1877 to 2016,
1003 observed levels, trends and uncertainties. *Elem Sci Anth*, 7(1), p.39. doi:<http://doi.org/10.1525/elementa.376>,
1004 2019b.
- 1005 Thomas, J. L., Raut, J.-C., Law, K. S., Marelle, L., Ancellet, G., Ravetta, F., Fast, J. D., Pfister, G., Emmons, L.
1006 K., Diskin, G. S., Weinheimer, A., Roiger, A., and Schlager, H.: Pollution trans- port from North America to
1007 Greenland during summer 2008, *Atmos. Chem. Phys.*, 13, 3825–3848, doi:10.5194/acp-13-3825- 2013,
1008 2013.
- 1009 Thomas, M. A., Devasthale, A., and Nygård, T.: Influence of springtime atmospheric circulation types on the
1010 distribution of air pollutants in the Arctic, *Atmos. Chem. Phys.*, 21, 16593–16608,
1011 <https://doi.org/10.5194/acp-21-16593-2021>, 2021.
- 1012 Thorp, T., Arnold, S. R., Pope, R. J., Spracklen, D. V., Conibear, L., Knote, C., Arshinov, M., Belan, B., Asmi,
1013 E., Laurila, T., Skorokhod, A. I., Nieminen, T., and Petäjä, T.: Late-spring and summertime tropospheric
1014 ozone and NO₂ in western Siberia and the Russian Arctic: regional model evaluation and sensitivities,
1015 *Atmos. Chem. Phys.*, 21, 4677–4697, <https://doi.org/10.5194/acp-21-4677-2021>, 2021.
- 1016 Tuccella, P., J. L. Thomas, K.S. Law, J.-C. Raut, L. Marelle, A. Roiger, B. Weinzierl, H. A. C. Denier van der
1017 Gon, H. Schlager, T. Onishi: Air pollution impacts due to petroleum extraction in the Norwegian Sea during
1018 the ACCESS aircraft campaign. *Elementa: Science of the Anthropocene*, University of California Press, 5,
1019 pp.25. (10.1525/elementa.124) . (insu-01538609) , doi:<https://doi.org/10.1525/elementa.124>, 2017.
- 1020 Turnock, S.T., O. Wild, A. Sellar and F.M. O'Connor: 300 years of tropospheric ozone changes using CMIP6
1021 scenarios with a parameterised approach, *Atmos. Environ.*, <https://doi.org/10.1016/j.atmosenv.2019.07.001>,
1022 2019.
- 1023 U.S. EPA (Environmental Protection Agency): Integrated Science Assessment for Ozone and Related
1024 Photochemical Oxidants. EPA/600/R-10/076F. Office of Research and Development, Research Triangle
1025 Park, NC (February), 2013.
- 1026 Van Dam, B., D. Helmig, P. V. Doskey, and S. J. Oltmans: Summertime surface O₃ behavior and deposition to
1027 tundra in the Alaskan Arctic, *J. Geophys. Res. Atmos.*, 121, 8055–8066, doi:10.1002/2015JD023914, 2016.
- 1028 Verstraeten, W. W., Boersma, K. F., Zörner, J., Allaart, M. A. F., Bowman, K. W., and Worden, J. R.:
1029 Validation of six years of TES tropospheric ozone retrievals with ozonesonde measurements: implications for
1030 spatial patterns and temporal stability in the bias, *Atmospheric Measurement Techniques*, 6, 1413–1423,
1031 <https://doi.org/10.5194/amt-6-1413-2013>, 2013.
- 1032 Viatte, C., Strong, K., Hannigan, J., Nussbaumer, E., Emmons, L. K., Conway, S., Paton-Walsh, C., Hartley, J.,
1033 Benmergui, J., and Lin, J.: Identifying fire plumes in the Arctic with tropospheric FTIR measurements and
1034 transport models, *Atmos. Chem. Phys.*, 15, 2227–2246, <https://doi.org/10.5194/acp-15-2227-2015>, 2015.
- 1035 Walker, T. W., et al.: Impacts of midlatitude precursor emissions and local photochemistry on ozone abundances
1036 in the Arctic, *J. Geophys. Res.*, 117, D01305, doi:10.1029/2011JD016370, 2012.
- 1037 Wang, S., & Pratt, K. A.: Molecular halogens above the Arctic snowpack: Emissions, diurnal variations, and
1038 recycling mechanisms. *Journal of Geophysical Research: Atmospheres*, 122, 11,991–12,007.
1039 <https://doi.org/10.1002/2017JD027175>, 2017.
- 1040 Wang, S. Y., S. M. McNamara, C. W. Moore, D. Obrist, A. Steffen, P. B. Shepson, R. M. Staebler, A. R. W.
1041 Raso and K. A. Pratt: Direct detection of atmospheric atomic bromine leading to mercury and ozone
1042 depletion, *Proceedings of the National Academy of Sciences of the United States of America* 116(29):
1043 14479–14484, 2019.
- 1044 Wespes, C., Emmons, L., Edwards, D. P., Hannigan, J., Hurt- mans, D., Saunois, M., Coheur, P.-F., Clerbaux,
1045 C., Cof- fey, M. T., Batchelor, R. L., Lindenmaier, R., Strong, K., Wein- heimer, A. J., Nowak, J. B.,
1046 Ryerson, T. B., Crounse, J. D., and Wennberg, P. O.: Analysis of ozone and nitric acid in spring and summer



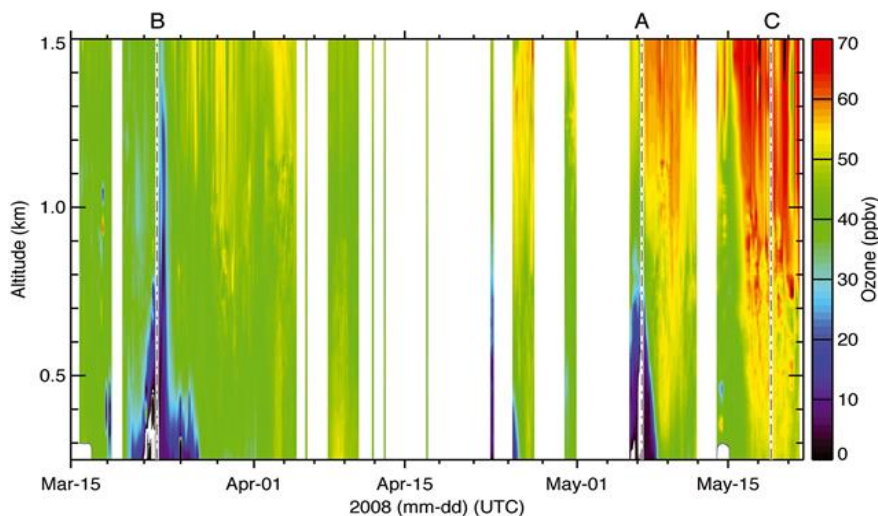
- 1047 Arctic pollution using aircraft, ground-based, satellite observations and MOZART-4 model: source
1048 attribution and partitioning, *Atmos. Chem. Phys.*, 12, 237–259, doi:10.5194/acp-12-237-2012, 2012.
- 1049 Whaley, C. H., R. Mahmood, K. von Salzen, B. Winter, S. Eckhardt, S. Arnold, S. Beagley, S. Becagli, R.-Y.
1050 Chien, J. Christensen, S. Manish Damani, X. Dong, K. Eleftheriadis, N. Evangeliou, G. Faluvegi, M.
1051 Flanner, J. S. Fu, M. Gauss, G. Giardi, W. Gong, J. Liengard Hjorth, L. Huang, U. Im, Y. Kanaya, S.
1052 Krishnan, Z. Klimont, T. Kuhn, J. Langner, K. S. Law, L. Marelle, A. Massling, D. Olivie, T. Onishi, N.
1053 Oshima, Y. Peng, D. A. Plummer, O. Popovicheva, L. Pozzoli, J.-C. Raut, M. Sand, L. N. Saunders, J.
1054 Schmale, S. Sharma, R. Skeie, H. Skov, F. Taketani, M. A. Thomas, R. Traversi, K. Tsigaridis, S. Tsyro, S.
1055 Turnock, V. Vitale, K. A. Walker, M. Wang, D. Watson-Parris, T. Weiss-Gibbons: Model evaluation of
1056 short-lived climate forcers for the Arctic Monitoring and Assessment Programme: a multi-species, multi-
1057 model study, *Atmos. Chem. Phys.*, in press, <https://doi.org/10.5194/acp-2021-975>, 2022.
- 1058 WHO (World Health Organization): Review of Evidence on Health Aspects of Air Pollution—REVIHAAP
1059 Project: Technical Report (Copenhagen: WHO Regional Office for Europe),
1060 [http://www.euro.who.int/data/assets/pdf_file/0004/193108/REVIHAAP-Final-technical-report-final-](http://www.euro.who.int/data/assets/pdf_file/0004/193108/REVIHAAP-Final-technical-report-final-version.pdf.2013)
1061 [version.pdf.2013](http://www.euro.who.int/data/assets/pdf_file/0004/193108/REVIHAAP-Final-technical-report-final-version.pdf.2013), 2013.
- 1062 Willis, M. D., Bozem, H., Kunkel, D., Lee, A. K. Y., Schulz, H., Burkart, J., Aliabadi, A. A., Herber, A. B.,
1063 Leaitch, W. R., and Abbatt, J. P. D.: Aircraft-based measurements of High Arctic springtime aerosol show
1064 evidence for vertically varying sources, transport and composition, *Atmos. Chem. Phys.*, 19, 57–76,
1065 <https://doi.org/10.5194/acp-19-57-2019>, 2019.
- 1066 Wofsy, S. C., S. Afshar, H.M. Allen, E.C. Apel, E.C. Asher, B. Barletta, J. Bent, H. Bian, B.C. Biggs, D.R.
1067 Blake, N. Blake, I. Bourgeois, C.A. Brock, W.H. Brune, J.W. Budney, T.P. Bui, A. Butler, P. Campuzano-
1068 Jost, C.S. Chang, M. Chin, R. Commane, G. Correa, J.D. Crouse, P. D. Cullis, B.C. Daube, D.A. Day, J.M.
1069 Dean-Day, J.E. Dibb, J.P. DiGangi, G.S. Diskin, M. Dollner, J.W. Elkins, F. Erdesz, A.M. Fiore, C.M.
1070 Flynn, K.D. Froyd, D.W. Gesler, S.R. Hall, T.F. Hanisco, R.A. Hannun, A.J. Hills, E.J. Hints, A. Hoffman,
1071 R.S. Hornbrook, L.G. Huey, S. Hughes, J.L. Jimenez, B.J. Johnson, J.M. Katich, R.F. Keeling, M.J. Kim, A.
1072 Kupc, L.R. Lait, J.-F. Lamarque, J. Liu, K. McKain, R.J. Mclaughlin, S. Meinardi, D.O. Miller, S.A.
1073 Montzka, F.L. Moore, E.J. Morgan, D.M. Murphy, L.T. Murray, B.A. Nault, J.A. Neuman, P.A. Newman,
1074 J.M. Nicely, X. Pan, W. Paplawsky, J. Peischl, M.J. Prather, D.J. Price, E.A. Ray, J.M. Reeves, M.
1075 Richardson, A.W. Rollins, K.H. Rosenlof, T.B. Ryerson, E. Scheuer, G.P. Schill, J.C. Schroder, J.P.
1076 Schwarz, J.M. St.Clair, S.D. Steenrod, B.B. Stephens, S.A. Strode, C. Sweeney, D. Tanner, A.P. Teng, A.B.
1077 Thames, C.R. Thompson, K. Ullmann, P.R. Veres, N. Vieznor, N.L. Wagner, A. Watt, R. Weber, B.
1078 Weinzierl, P.O. Wennberg, C.J. Williamson, J.C. Wilson, G.M. Wolfe, C.T. Woods, and L.H. Zeng.: ATom:
1079 Merged Atmospheric Chemistry, Trace Gases, and Aerosols, Ornl Daac, Oak Ridge, Tennessee, USA.
1080 <https://doi.org/10.3334/ORNLDAAAC/1581>, 2018.
- 1081 Yang, X., Blechschmidt, A.-M., Bogner, K., McClure–Begley, A., Morris, S., Petropavlovskikh, I., Richter, A.,
1082 Skov, H., Strong, K., Tarasick, D., Uttal, T., Vestenius, M., and Zhao, X.: Pan-Arctic surface ozone:
1083 modeling vs measurements, *Atmos. Chem. Phys.*, 20, 15937–15967, <https://doi.org/10.5194/acp-2019-984>,
1084 2020.
- 1085 Young, P. J., V. Naik, A. M. Fiore, A. Gaudel, J. Guo, M. Y. Lin, J. L. Neu, D. D. Parrish, H. E. Rieder, J. L.
1086 Schnell, S. Tilmes, O. Wild, L. Zhang, J. R. Ziemke, J. Brandt, A. Delcloo, R. M. Doherty, C. Geels, M. I.
1087 Hegglin, L. Hu, U. Im, R. Kumar, A. Luhar, L. Murray, D. Plummer, J. Rodriguez, A. Saiz-Lopez, M. G.
1088 Schultz, M. T. Woodhouse and G. Zeng: Tropospheric Ozone Assessment Report: Assessment of global-
1089 scale model performance for global and regional ozone distributions, variability, and trends, *Elem Sci Anth.*,
1090 6(1):10. DOI: <http://doi.org/10.1525/elementa.265>, 2018.
- 1091 Zanis, P., D. Akritidis, S. Turnock, V. Naik, S. Szopa, A. K. Georgoulas, S. E. Bauer, M. Deushi, L. W.
1092 Horowitz, J. Keeble: Climate change penalty and benefit on surface ozone: a global perspective based on
1093 CMIP6 earth system models, *Environ. Res. Lett.*, 17, 024014, <https://doi.org/10.1088/1748-9326/ac4a34>,
1094 2022.
- 1095 Zheng, C., Wu, Y., Ting, M., Orbe, C., Wang, X., & Tilmes, S.: Summertime transport pathways from different
1096 northern hemisphere regions into the Arctic. *Journal of Geophysical Research: Atmospheres*, 126,
1097 e2020JD033811. <https://doi.org/10.1029/2020JD033811>, 2021.



1098 Zhu, L., E. V. Fischer, V. H. Payne, J. R. Worden, and Z. Jiang: TES observations of the interannual variability
1099 of PAN over Northern Eurasia and the relationship to springtime fires, *Geophys. Res. Lett.*, 42, 7230–7237,
1100 doi:10.1002/2015GL065328, 2015.

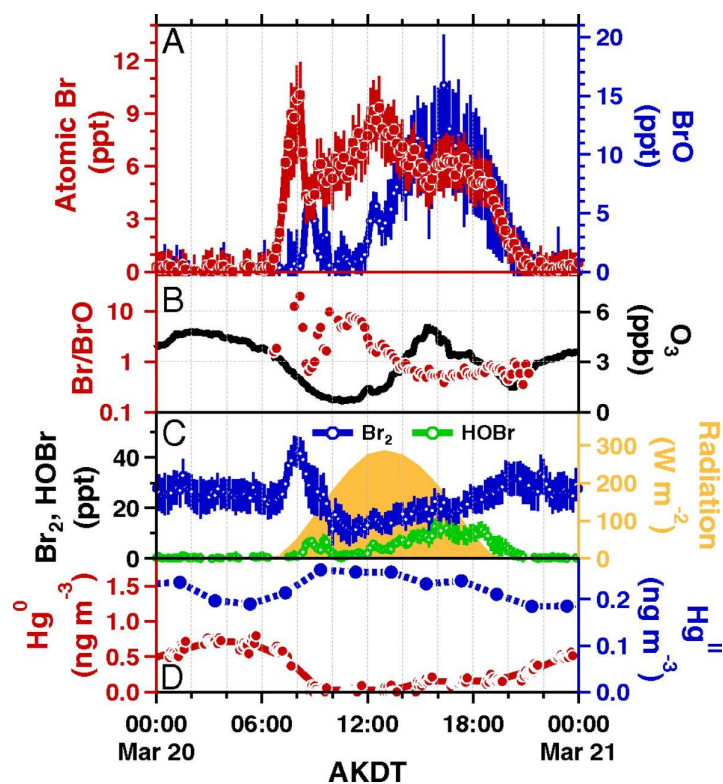


1101
1102 **Figure 1:** Schematic of Arctic tropospheric O₃ sources, sinks, and relevant processes.



1103
1104 **Figure 2:** Ozone lidar measurements from Eureka in the spring of 2008 showing effects of large-scale
1105 meteorology including low O₃ in the lower troposphere when air masses originate from the north over the Arctic
1106 Ocean and enhanced O₃ during downward transport into the Arctic boundary layer when the airflow was from
1107 the south over mountains. From Figure 3 in Seabrook and Whitway (2016), *JGR Atmospheres*, vol. 121, Issue:
1108 4, Pages: 1935-1942, First published: 04 February 2016, DOI: (10.1002/2015JD024114)

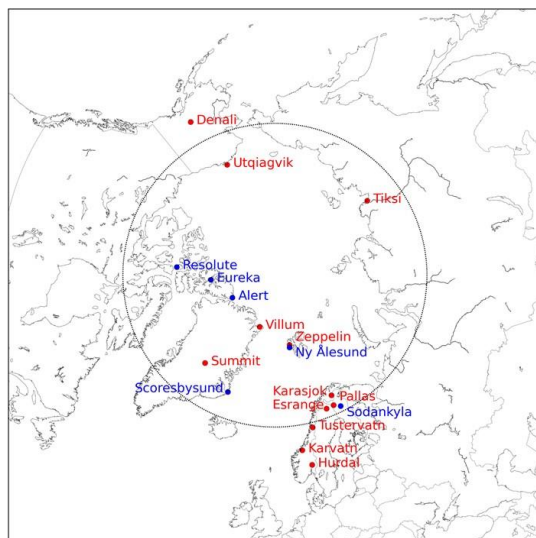
1109



1110

1111 **Figure 3:** Time series at Uqiagvik on 20 March 2012 of measured (A) atomic bromine (Br) and bromine
1112 monoxide (BrO), (B) Br/BrO ratios and O₃. Error bars represent propagated measurement uncertainties. Figure
1113 based on Wang et al. (2019, PNAS). (EPS figure provided for the report). From Figure 2 in Wang et al. (2019),
1114 PNAS, vol. 116, no. 29, pages 14479-14484, Copyright (2019) National Academy of Sciences.

1115

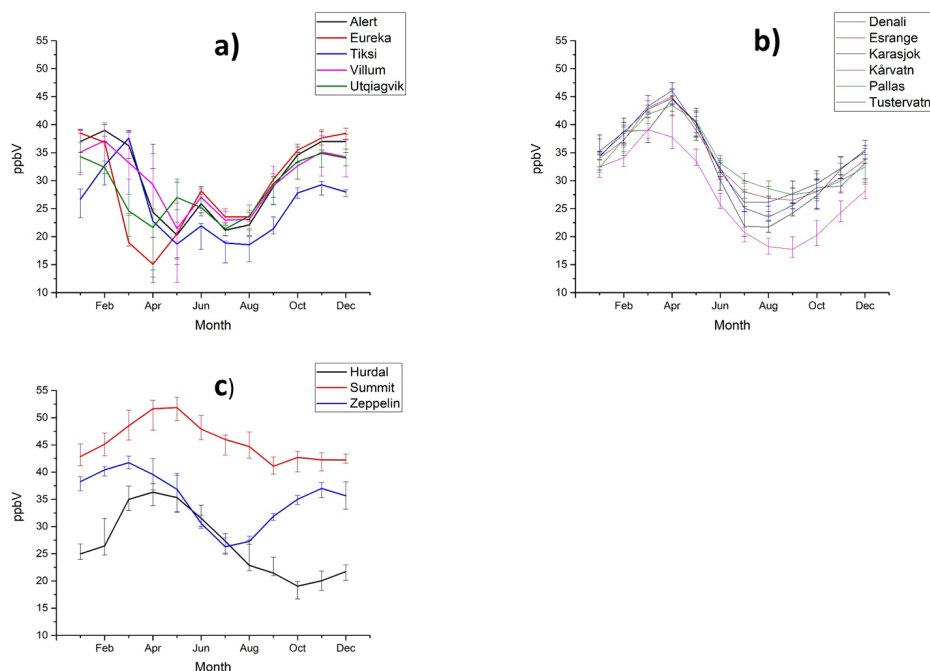


Name	Longitude	Latitude	Elevation (msl)
Alert	-62.33	82.50	66
Denali	-151.19	63.11	660
Esrange	21.07	67.88	475
Eureka	-86.4	80.1	83
Hurdal	11.07	60.44	300
Karasjok	25.22	69.47	333
Karvatn	8.88	62.78	210
Pallas	24.25	67.97	565
Summit	-38.48	72.57	3211
Tiksi	128.9	71.6	10
Tustervatn	13.87	65.83	439
Utqiagvik	-156.61	71.32	11
Villum	-16.67	81.60	20
Zepelin	11.89	78.91	474
Ny Alesund	11.49	78.51	
Resolute	-94.82	74.68	
Scoresbysund	-21.97	70.48	
Sodankyla	26.65	67.37	

1116

1117 **Figure 4.** Map of the surface (red) and ozonesonde (blue) sites, cited in the present study, with coordinates and
 1118 elevation. Eureka and Alert are both surface and soundings sites. ‘Utqiagvik’ was formerly called ‘Barrow’.

1119 The Arctic Circle at 66.55° N is also shown in the figure for reference.

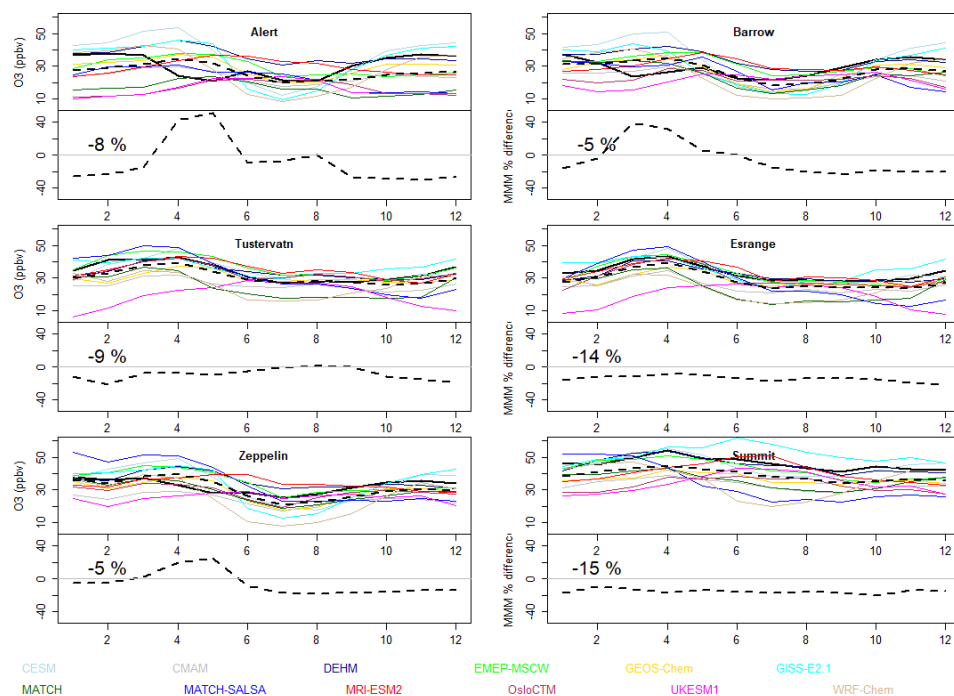


1120

1121 **Figure 5:** Seasonal behavior of surface O₃ at selected Arctic stations that are representative of a) coastal high
 1122 Arctic b) near Arctic Circle and c) inland and high-elevation sites. Monthly medians are calculated for the period
 1123 2003 to 2018. Data were not available for Villum and 2004 and 2013-2015 for Alert. The
 1124 error bars show upper (75%) and lower (25%) quartiles.



1125



1126

1127 **Figure 6:** Arctic surface O₃ by month; seasonal cycle model comparisons. Top row: coastal high-Arctic sites;

1128 middle row: near-Arctic circle sites; bottom row: high elevation sites. The solid black line is the observed O₃

1129 monthly means, and the dashed black line is the multi-model median. Bottom row: sub-panels show the MMM

1130 % difference [(MMM - measurements)/measurements*100].

1131 *Note model results are from the 2014-15 mean. When available, the same years are used for the observations.

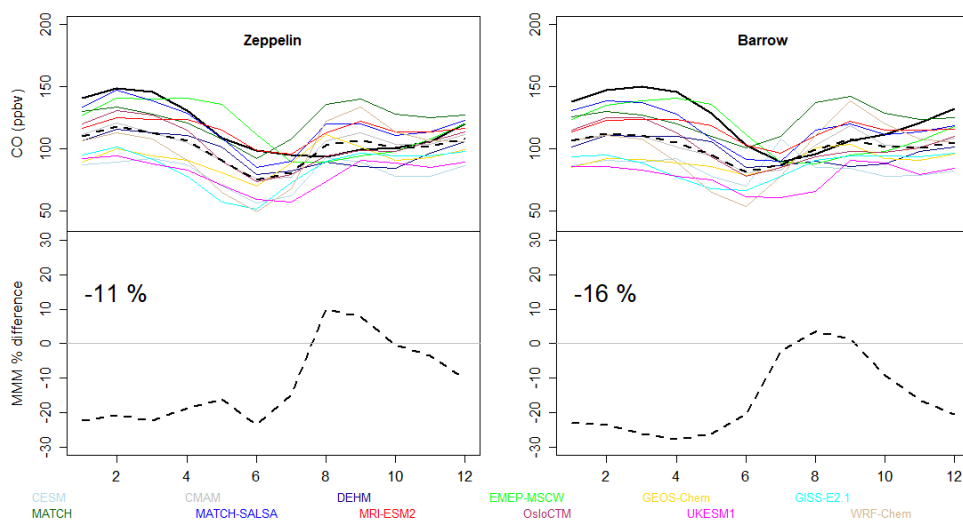
1132 However, Alert did not have data for 2014-15, so its most recent years were used: 2010-2013. Summit had 2014,

1133 but only 1 month in 2015, so its 2013-2015 data were used.

1134

1135

1136



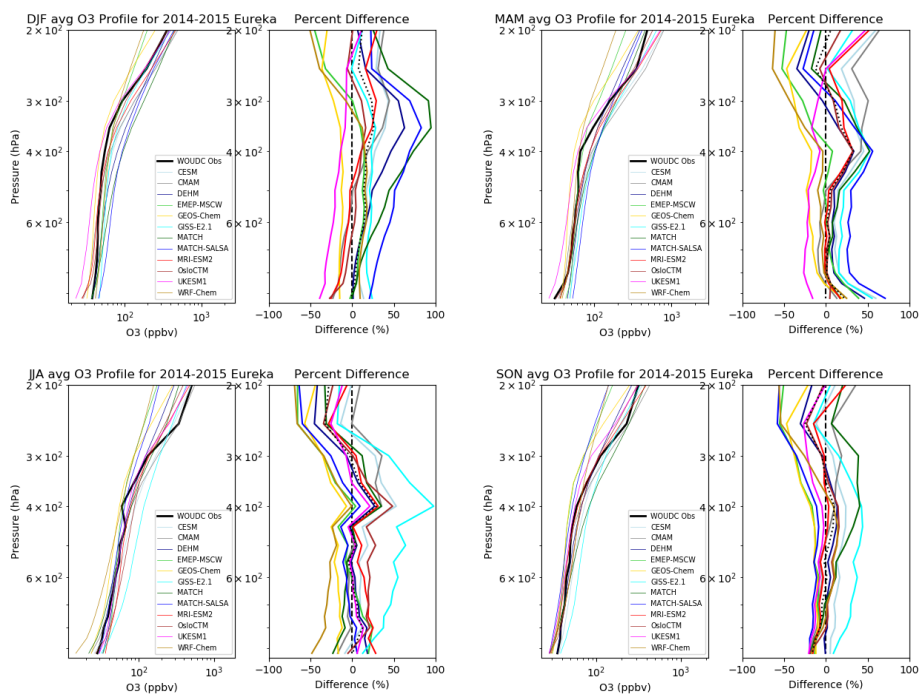
1137

1138 **Figure 7:** Arctic surface CO by month; seasonal cycle model comparisons. The solid black line is the observed
1139 CO monthly means, and the dashed black line is the multi-model median (MMM). Bottom panels show the
1140 MMM % difference $[(\text{MMM} - \text{measurements})/\text{measurements} \times 100]$.

1141 *Note model results are from the 2014-15 mean. When available, the same years are used for the observations.

1142 However, for Zeppelin observations are the mean of 2013-14.

1143



1144

1145

1146

Figure 8: Comparison between observed (thick black line on left panels) and AMAP models' (colored lines) O₃ seasonal averages for 2014-15 at Eureka, NV, Canada. These use monthly mean model output. On each right panel, the dotted black line is the MMM, and the dashed black line shows zero bias for reference. See supplement (Figure S.1) for the rest of the ozonesonde locations, and a sample comparison done with 3-hourly model output (Figure S.2).

1151

1152

1153

1154

1155

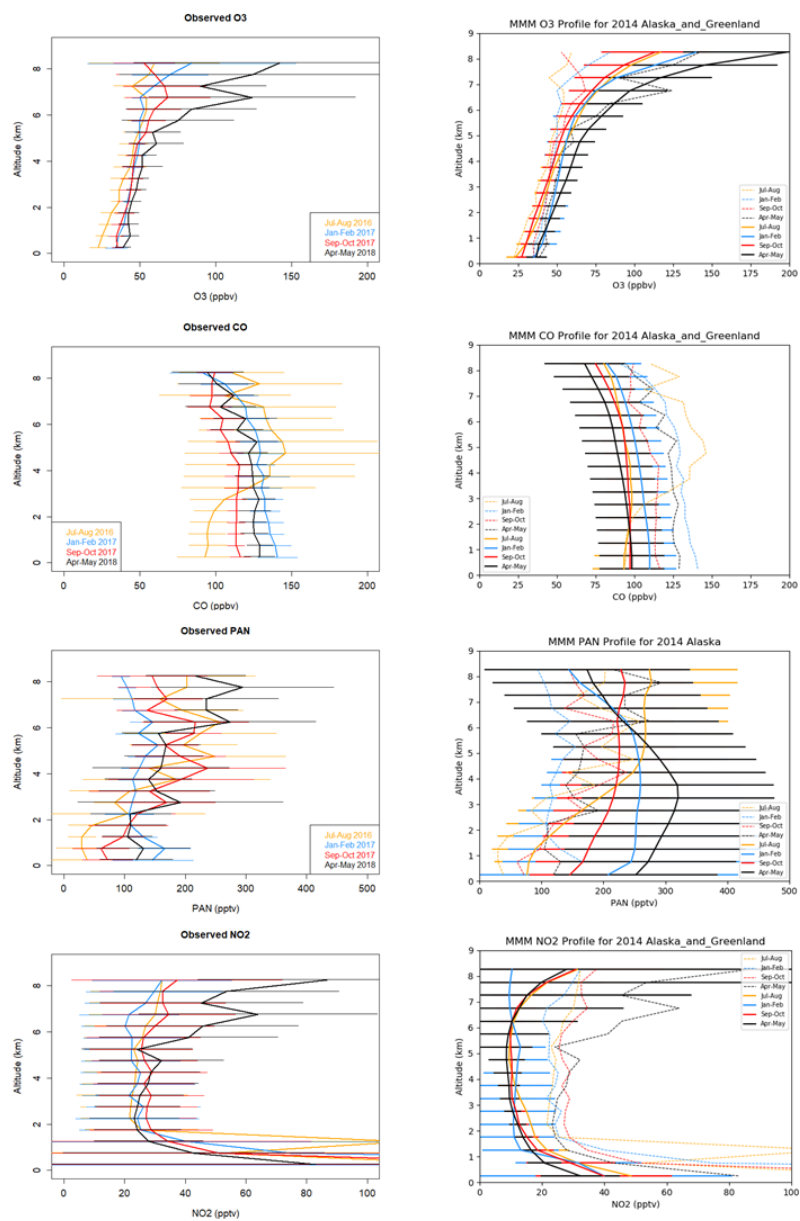
1156

1157

1158

1159

1160



1161

1162 **Figure 9:** Mean vertical profiles of O₃, CO, PAN and NO₂ (**left**) measured in Alaska and Greenland from the
1163 NASA ATom missions during summer 2016, winter 2017, autumn 2017 and spring 2018 (horizontal lines
1164 indicate 1 standard deviation spread around mean values at each altitude. (**right**) the MMM for the years 2014-
1165 15 (with the MMM standard deviation as horizontal lines). The observations appear as dashed lines in the right
1166 panels, for ease of comparing to the MMM.